

NLSEmagic: Nonlinear Schrödinger Equation Multidimensional Matlab-based GPU-accelerated Integrators using Compact High-order Schemes

R. M. Caplan

March 9, 2022

Abstract

We present a simple to use, yet powerful code package called NLSEmagic to numerically integrate the nonlinear Schrödinger equation in one, two, and three dimensions. NLSEmagic is a high-order finite-difference code package which utilizes graphic processing unit (GPU) parallel architectures. The codes running on the GPU are many times faster than their serial counterparts, and are much cheaper to run than on standard parallel clusters. The codes are developed with usability and portability in mind, and therefore are written to interface with MATLAB utilizing custom GPU-enabled C codes with the MEX-compiler interface. The packages are freely distributed, including user manuals and set-up files.

1 Introduction

The nonlinear Schrödinger equation (NLSE) is a universal model describing the evolution and propagation of complex field envelopes in nonlinear dispersive media. As such, it is used to describe many physical systems including Bose-Einstein condensates [2], nonlinear optics [3], the evolution of water waves, thermodynamic pulses, nonlinear waves in fluid dynamics, and waves in semiconductors [1]. The general form of the NLSE can be written as

$$i \frac{\partial \Psi}{\partial t} + a \nabla^2 \Psi - V(\mathbf{r}) \Psi + s |\Psi|^2 \Psi = 0, \quad (1)$$

where $\Psi(\mathbf{r}, t) \in \mathbb{C}$ is the value of the wavefunction, $\nabla^2 = \frac{\partial^2}{\partial x^2} + \frac{\partial^2}{\partial y^2} + \frac{\partial^2}{\partial z^2}$ is the Laplacian operator, and where $a > 0$ and s are parameters defined by the system being modeled. $V(\mathbf{r})$ is an external potential term, which when included, makes Eq. (1) known as the Gross-Pitaevskii equation [2].

Since the NLSE is nonlinear, many of the most interesting dynamical solutions do not have a closed form and require the use of direct numerical simulations. Often, researchers will produce codes to accomplish this which, after the project is completed, are never used again. Thus, other researchers in the field must produce their own codes, a classic case of re-inventing the wheel. Although every problem is different, we feel that producing a freely distributed code package that is powerful and easy to use will help a wide range of researchers in the field, especially since the codes are easily altered to conform to the specific problem and model equations of the user.

Many interesting problems (especially those in high dimensions) require very large simulations. In such cases, it is desirable to use code run on parallel computational systems that can greatly reduce the simulation time. Generally, this means running codes on expensive large clusters of PCs through the MPI and/or OpenMP application programming interface s (APIs). However, recently

a new breed of parallel computing has been gaining great interest, that of general purpose graphical processing units (GPUs).

Graphical processing units were first developed in order to allow graphics cards to parallelize their massive computations to speed up video games and image processing. It was then realized that such hardware could be adapted to run scientific codes as well. This led to the development of code APIs which allows one to write code which takes advantage of the GPU hardware. NVIDIA cooperation is the leading company in this new form of computing, developing the compute unified device architecture (CUDA) API which can be compiled to run scientific codes on NVIDIA's line of GPU video cards, as well as non-video stand-alone GPUs designed specifically for parallel computation.

For many problems, GPU computing is seen as a large improvement over previous parallel techniques. A typical GPU (as of this writing) can have up to 1024 processing cores and up to 6GB of RAM, with a throughput of over a Tera-FLOP on a single card. The price of the GPUs is another major factor, as one (as of this writing) can purchase an off-the-shelf GPU with over 400 cores, and 2GB of RAM for under \$450. This allows for super-computing capabilities to be realized on a single desktop PC.

Since access to a large cluster can be expensive or not available, we have written NLSEmagic to use GPU accelerated finite-difference integrator codes in C using CUDA. GPUs have been used for various finite-difference scheme codes with good results [4–9]. In Ref. [4], the authors wrote code to simulate the two-dimensional Maxwell equations yielding a speedup of up to ten times when compared to the CPUs of the day (2004). They did this before CUDA was developed using basic assembly code directly. Ref. [5] also did not utilize CUDA for their simulations of the 3D Maxwell equations. Speedups of over 100 times were reported. The 2D Maxwell equation was simulated in Ref. [6] using CUDA code where speedups of 50 were reported. In Ref. [7], the authors simulate the 3D wave equation with an eighth-order finite-difference scheme using CUDA on multiple GPUs. A similar multi-GPU code was shown in Ref. [8] for the 3D wave equation using a fourth-order finite-difference scheme where speedups of 60 were reported. In Ref. [9], the authors use CUDA to simulate the multi-dimensional complex Ginzburg-Landau equation (a generalization of the NLSE), but speedups versus CPU codes were not reported as their main goal was to compare the CUDA codes using a complex structure versus using explicit treatment of the real and imaginary part of the solution.

MATLAB is a mathematical computational software program created by MathWorks Inc. It has become a standard in many academic institutions as well as in industry for mathematical computations. However, there is a prevalent opinion that while MATLAB may be useful for course work, small-scale codes, and learning purposes, for serious calculations it is simply too slow to be useful. We show that this is not the case, and as such, one can take advantage of all the benefits and ease of using MATLAB while still running large efficient codes. This makes numerical studies much more efficient as visualizations, formation of initial conditions, optimizations, and analysis of data become much easier to implement and eliminate the need for post-processing in most cases.

The way to achieve efficient large-scale codes in MATLAB is to write custom C codes which connect to MATLAB through an interface compiler called MEX. Once the C codes have been written to be MEX-compatible and compiled, they can be called from a MATLAB script directly. The codes run as fast as an equivalent stand-alone C code, with minimal overhead, and are up to 10 times faster than the equivalent script codes.

Since the native language for GPU-compatible CUDA codes is C, adding GPU functionality to MATLAB is in theory straightforward (however setup can be difficult, an issue addressed in Sec. 8). The newest versions of MATLAB have GPU-compatibility built-in [10], and ways to

compile CUDA C code segments into callable functions. However, because many researchers do not have the newest versions of MATLAB, in the interest of portability, it is preferable to not use these built-in functions, but rather write C codes which contain CUDA code directly, and compile them with a CUDA-capable MEX compiler called NVNEX [11]. Further portability is maintained in this manner by noting that besides the initial MEX interface in the C codes (which gives the code access to the MATLAB input parameters and data), the codes are written in generic C and CUDA C code, which can easily be exported to a purely C code if desired.

The NLSEmagic integrator codes utilize fully explicit finite-difference schemes, meaning that the solution at the next time-step only relies on values of the solution at the previous time-step. This eliminates the need for solving linear systems and nonlinear iterations at each time-step (which most implicit schemes do). The drawback is that a conditional stability exists that limits the time-step size based on the spatial grid-spacing and the scheme used to approximate the spatial derivatives. This relationship is discussed in Sec. 3.4, and is hard-coded into the driver scripts of NLSEmagic. The spatial schemes used are a standard second-order central difference and a new two-step high-order compact scheme which is fourth order accurate.

This paper is organized as follows: In Sec. 2, we describe general purpose GPUs, specifically NVIDIA brand GPUs. We discuss the physical structure of the GPUs as well as the CUDA API logical structure. Compatibility and portability issues are also discussed. In Sec. 3, we discuss the numerical algorithms used in NLSEmagic including boundary conditions and stability. The example solutions to the NLSE that are used throughout the simulations in this paper are described in Sec. 4. The serial code implementation of the integrators is described in Sec. 5, including the script integrators and a detailed description of the MEX code integrators. Speedup results between the MEX codes and the equivalent C codes are shown. Sec. 6 describes in detail our implementation of the NLSEmagic integrators in CUDA MEX codes. The speedup results of the CUDA MEX codes compared to the equivalent serial MEX codes are shown in Sec. 7. An overview of the NLSEmagic code package is described in Sec. 8 including distribution details.

2 General Purpose GPU Computing with NVIDIA GPUs

Although there are other companies that produce GPU graphics cards (such as ATI), NVIDIA is by far the most established when it comes to general-purpose GPUs. Their compute-only Tesla general purpose GPU (GPGPU) cards as well as their native CUDA API and enormous support and development infrastructure make NVIDIA the most logical choice for developing and running GPU codes (compatibility and portability concerns will be discussed in Sec. 2.4). In this section we describe the physical structure of the GPUs as well as the logical structure defined in the CUDA API.

2.1 NVIDIA GPU Physical Structure

Since the programming model for NVIDIA GPUs is very closely related to their physical design, it is important to have an overview of the physical structure of the GPUs. Also, because NVIDIA produces several different models and architectures, a description of these varieties is important for proper implementation of GPU codes.

The typical GPU is a separate piece of hardware that is connected to the PC through a PCIe slot. However, NVIDIA also makes built-in GPU motherboards, as well as integrated GPUs for laptop computers. A simplified schematic of a current-model (Fermi architecture) NVIDIA GPU is shown in Fig. 1. The GPU contains a number of stream multiprocessors (SM) which each contain

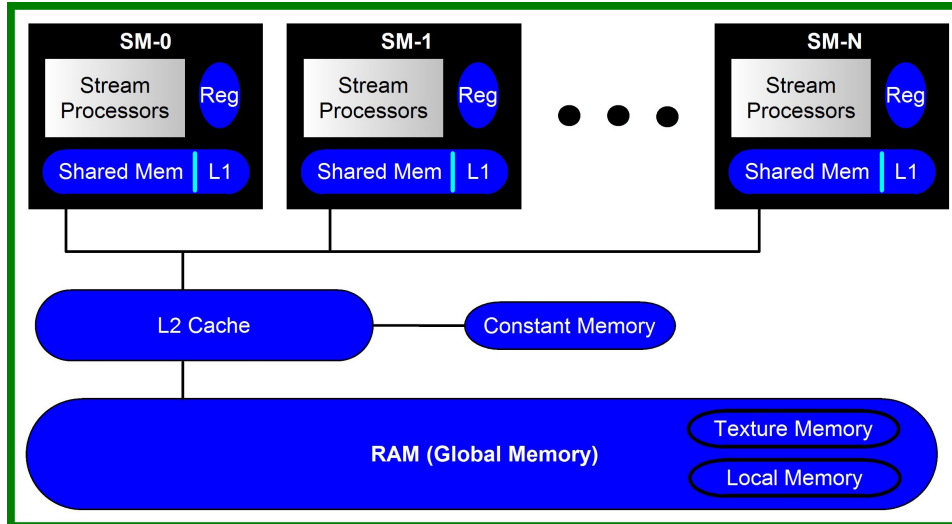


Figure 1: Simplified schematic of NVIDIA GPU with Fermi architecture (Tesla architecture looks the same but without caches).

a number of stream processors (SP) which are the compute cores of the GPU. Each SM performs computations independently and simultaneously from the other SMs and has no connectivity or communication with other SMs. Each SM has a small, fast memory which is configured to allocate some space for a level 1 (L1) cache and the rest of the space for shared memory. The shared memory is shared between all SPs, so each core can access any part of shared memory. Each SM also has fast registers for the SPs to use for computations and storage of local variables.

The main memory of the GPU is a large amount of DRAM called the global memory space which, depending on the GPU, can have a capacity from 512MB up to 12GB. Accesses to the global memory from the SPs are two orders of magnitude slower than accesses to shared or constant memory [12] (an additional small [64KB] globally-accessible memory space which is as fast as shared memory). Parts of the global memory space are used for local variables (when they cannot fit into registers or cache) and texture memory which is mainly only allocated for graphics processing. Between the DRAM and the SMs is a level 2 (L2) cache which improves memory performance when SMs access global memory. Additional hardware details are beyond the required scope of this paper.

A typical GPU code transfers data from the host computer’s RAM to the GPU RAM, performs computations using the data on the SMs of the GPU, and then when completed, transfers the resulting data back to the host computer’s RAM. The memory transfer has large latency associated with it, and so it is ideal to compute as much as possible on the GPU before transferring the data back. However, since the host computer cannot ‘see’ the data until it has been transferred back from the GPU, a trade-off between maximum performance and usability is often encountered. However, for many applications (including NLSEmagic), this issue is easily resolved (see Sec. 7.1).

An additional issue to keep in mind is that if one is using a video-enabled GPU, there is a run-time limit on individual GPU function calls. Each call to an executable GPU routine cannot take more than the display driver timeout limit of the operating system (typically a few seconds) to compute, otherwise the display driver will shut down and reset. This is usually not a problem because most GPU codes (including NLSEmagic) run many small GPU function calls, each of

which take less than the run-time limit to compute. However, if the run-time limit does become a problem, one can simply run the codes on a compute-only GPU.

The first general purpose GPUs developed by NVIDIA utilized a chipset design called the Tesla architecture. The design was similar to that of Fig. 1, except that there were no caches. Each SM had 8 SPs and 16KB of shared memory. The ALUs of the SPs were not fully IEEE compliant which meant that results computed on the GPU could differ slightly from those computed on a CPU. Double-precision arithmetic was not supported in early models, but was later added (again, not fully IEEE compliant). The global memory RAM did not have ECC error correction.

The newest generation of NVIDIA GPUs implement a chipset called the Fermi architecture. The Fermi-based cards are a large improvement over the older Tesla-based cards. Some of the key improvements are [13]:

- Addition of an L1 and L2 cache system which helps reduce memory latency.
- ECC error-correcting memory (not available on GeForce model cards, see below).
- More SPs (cores) per SM (24-32), and more total SPs possible (up to 1024).
- Fully IEEE compliant floating-point operations.
- Amount of shared memory per SM increased to up to 48KB (instead of 16KB).
- Amount of compute threads increased from 512 to 1024 threads per block (see Sec. 2.2).

NVIDIA produces three GPU product lines which now all use the Fermi architecture. These are GeForce, Quadro, and Tesla (not to be confused with the Tesla *architecture*). The GeForce GPUs are graphics cards targeted towards gamers, the Quadro GPUs are graphics cards targeted towards professional graphic workstations, and the Tesla line of GPUs are compute-only devices with no display output targeted for scientific applications. Both the Quadro and Tesla cards are much more expensive than the comparable GeForce cards.

The basic internal chipset of the GeForce cards are the same as the Tesla cards with a few important differences [14]. The double precision arithmetic performance has been artificially reduced to 25% of the Tesla cards, and the ECC error correction is disabled and cannot be enabled. However, the ECC memory option reduces performance and available memory when activated, and in many simulations, the order of accuracy is not sensitive enough to be effected by the lack of ECC memory. GeForce GPUs also tend to come with less global RAM than the Tesla or Quadro cards. In addition, the Tesla cards have two copy engines, while the GeForce cards have one. This means that CUDA codes run on the Tesla cards can simultaneously compute and transfer memory to the CPU which increases performance. Tesla cards are also built with higher standards than GeForce cards, and are put through a zero-error tolerance stress test and burn-in. For all these reasons, Tesla cards are more desirable than GeForce cards for serious codes. However, for moderate problems, the GeForce's abilities are often more than adequate, and their low price-tag makes them an affordable option for high-performance computing.

The current top of the line Fermi-based card for home PC use is the GeForce GT 590 which has 1024 compute cores and 3GB RAM and costs approximately \$750. The current top Tesla card is the M2090 with 512 cores and 6GB memory and costs around \$4000, while the current top-of-the-line Quadro card is the Quadro Plex 7000 with 1024 cores and 12GB RAM and sells for around \$14,000.

2.2 CUDA API and Logical Structure

NVIDIA allows programmers to utilize its GPUs through an API called the compute unified device architecture (CUDA) API. CUDA is a code extension to C/C++ which gives low-level access to the GPUs memory and processing abilities. The CUDA codes are compiled by a provided compiler called `nvcc`.

There are two sections of a CUDA C code (usually written in a file with a `.cu` extension). One section of code is the host code which is executed on the CPU. This section contains setup commands for the GPU, data transfer commands to send data from the CPU to the GPU (and vice-versa), and code to launch computations on the GPU. The second part of a CUDA code contains what are known as CUDA kernel routines. These are routines which get compiled into binaries which are able to be executed on the GPU by calls evoked by the host code.

The CUDA programming model is based on a logical hierarchical structure of grids, blocks, and threads. This hierarchy is shown in Fig. 2. When a kernel is launched, it is launched on a user-

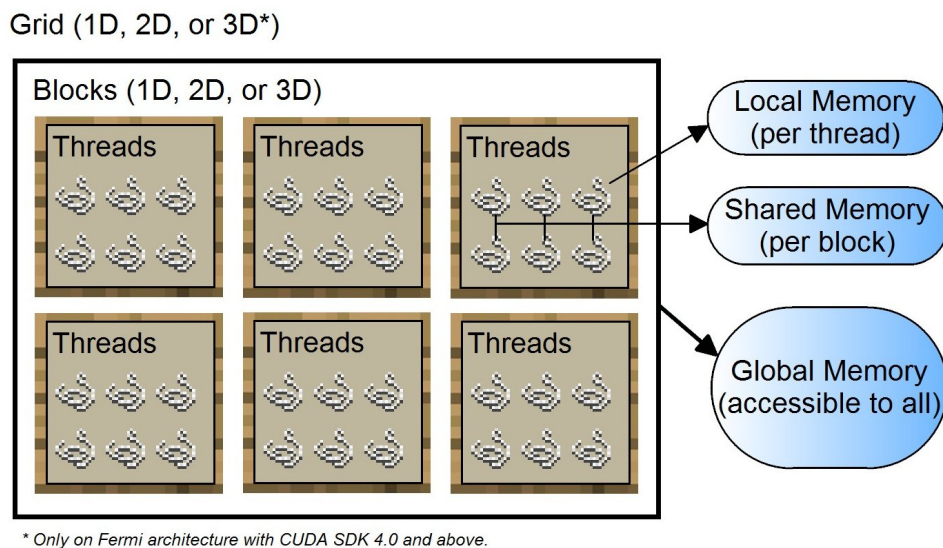


Figure 2: Schematic of CUDA API logic structure.

defined compute-grid which can be one-, two-, or three-dimensional (three-dimensional compute-grids are only available on Fermi architecture with the CUDA SDK 4.0 or above installed). This grid contains a number of blocks. The computations to be performed are distributed over the blocks. Each block must be able to compute independently and no synchronization is possible between blocks. Each block contains a number of threads, which are laid out in a configuration that is one-, two-, or three-dimensional. The threads are what perform the computations and multiple threads are computed simultaneously on the SM. Synchronization of threads within a block is possible, but for best performance, should be kept to a minimum. Each thread has its own local memory and all threads in a block have access to a shared memory. All threads in all blocks on the grid have access to the global memory. Each thread has access to intrinsic variables (stored in registers) which are used to identify its position in the compute-grid and block. The grid dimensions are stored in variables called `gridDim.x`, `gridDim.y`, and `gridDim.z` and the block dimensions are stored in `blockDim.x`, `blockDim.y`, and `blockDim.z`. The block that a thread is contained in is given in coordinates by the variables `blockIdx.x`, `blockIdx.y`, and (for Fermi cards

with SDK 4.0 and above) `blockIdx.z`. The thread's position in the block is given by the variables `threadIdx.x`, `threadIdx.y`, and `threadIdx.z`. All these variables are used to determine what part of the problem the specific thread computes.

The logical structure relates directly to how the hardware of the GPU executes a kernel code. Each block is executed by an SM, where each thread is executed by an SP. This is why the threads within a block have access to a shared memory, but blocks cannot access each others shared memory. The local memory of each thread is stored in the registers of the SM, unless the register space is used up in which case the local variables get stored in cache, and, if the cache's are full, to global memory.

2.3 Compatibility

Since new and updated GPU cards are being developed and released continuously, compatibility can become a major concern. To help with this issue, NVIDIA has maintained a compatibility scheme known as the major/minor compute capability of a GPU. This is a number in the form of $y.x$ where y and x are the major and minor compute capabilities respectively. Whether code written and compiled for one GPU will work on a different model GPU depends on the compute capabilities of the two cards and on how the code was compiled.

CUDA codes can be compiled into a binary executable for a specific GPU known as 'cubin' objects, and/or be compiled into parallel thread execution (PTX) assembly code which are compiled into binary at runtime for the GPU being used. Each compilation scheme has separate compatibility rules.

Codes compiled into a cubin object are only compatible with future minor compute capability revisions. Therefore, for example, a cubin file compiled for compute capability 1.2 will run on CUDA cards with compute capabilities 1.2 and 1.3, but not with those of 1.1 or 2.0. In contrast, codes compiled into PTX assembly code are compatible with *any* future compute capability. However, features that are present in higher compute capabilities cannot be used by previous PTX codes. For example, double precision is only supported in GPUs with compute capabilities of 1.3 and above. Therefore, if one has CUDA code which uses double precision, they must compile the PTX codes using compute capability 1.3. If not, (say, compiling for PTX code of 1.0), the double precision gets demoted to single precision. A drawback of using PTX codes is that they increase the load time of the application due to the in-time compilation (although typically after the first compile, the binary is stored in a cache for future runs of the application) [12].

The compiler options for NLSEmagic have been set to compile PTX code for 1.0, 1.3, and 2.0, as well as cubin objects for compute capability 2.0 (the major compute capability 2.x is Fermi architecture, while 1.x is Tesla). This ensures that the current form (Fermi-optimized) codes can compile (trying to compile to cubin files for old architecture fails when using new features such as larger shared memory and double precision).

To use NLSEmagic with older GPUs (lower than 2.0 compute capability), one must make minor modifications to some of the CUDA integrator codes and recompile them. The block sizes (in the .cu files as well as the driver scripts) must be altered so that there are less than 512 threads per block, and that the total shared memory per block is less than 16KB. Also, the double precision codes will not work with GPUs with compute capabilities less than 1.3. Additionally, for efficiency, the `nvmexopts(64).bat` or `nvopts.sh` (see Sec. 8) should be altered to compile native cubin objects for the specified architectures compute capability level in order to avoid the loading delay of the in-time compilation of PTX codes.

2.4 Portability

A major reason many scientific programmers are hesitant to write their programs for GPUs and using CUDA to do so, is the issue of portability. The concern is that one could spend years developing GPU codes with CUDA only to find out that the GPUs have been replaced with alternate technology and are no longer supported, or, that another company has overtaken the GPU market and NVIDIA’s native CUDA API is no longer being supported (although this seems unlikely).

As a solution to these concerns, a new API called OpenCL [15] has been developed by the Khronos Group [16] which can function across multiple GPU vendors, as well as other CPU architectures. Although code written in OpenCL is guaranteed to work on all multi-core architectures, specific optimization is necessary for the codes to work efficiently. A number of studies have been done comparing the performance of OpenCL versus CUDA [17–19]. In general, the CUDA codes outperform the OpenCL equivalent codes (sometimes by a significant percentage). However, with further OpenCL-specific performance tunings, it is possible to get the OpenCL codes to run nearly as fast as the CUDA codes. OpenCL and CUDA are very similar in terms of logical structure and code design. Therefore, codes written in CUDA can easily be changed into OpenCL codes (in fact, an *automatic* CUDA-to-OpenCL converter called `cu2c1` has recently been developed [20]).

Another option for portability is the Portland Group’s new x86 CUDA compiler [21]. This allows the compilation of CUDA codes into binaries that are able to be run on multi-core x86 CPUs (with 64-bit support being developed). This will allow CUDA codes to be useful even if GPUs are overtaken by multi-core CPUs in the market.

Similar to the x86 compiler is the MCUDA compiler created by the University of Illinois at Urbana-Champaign Center for Reliable and High-Performance Computing [22]. This compiler can take CUDA code and automatically convert it into pure C code that interfaces to a runtime library for parallel execution on multi-core PCs through the use of POSIX threads.

Another portability option is the Ocelot project from Georgia Tech [23] which allows CUDA codes that have been compiled into PTX code to be run on AMD GPUs as well as CPU architectures without needing to recompile the codes. This would directly allow one to continue using CUDA codes on alternative hardware.

For developers who are still unsure about putting the time in to make CUDA codes, NVIDIA has recently announced a new compiler developed by the Portland Group which can compile a previously written serial C code and, with a few helper-comments, compile the code to run on a GPU automatically with no direct CUDA programming [24]. Although it is expected that the resulting code will exhibit much less speedup than directly coding the CUDA by hand, NVIDIA has guaranteed at least a 2X speedup when using the new compiler.

From the numerous portability options, we conclude that there is little risk in taking the time to develop GPU codes using CUDA, and the potential speedup of the codes far outweighs any risk. Therefore, we use CUDA to write our NLSE integrators in NLSEmagic.

3 Finite-Difference Schemes

There are many ways to numerically integrate the NLSE. The scheme we use is the classic fourth-order Runge-Kutta (RK4) in time and a choice of either a standard second-order central-difference (CD) in space for the Laplacian operator, or a new fourth order two-step high order compact scheme (2SHOC) [25]. These schemes are some of the simplest explicit finite-difference schemes for the NLSE that are conditionally stable. Once the principles of the CUDA implementation are understood, more advanced schemes could be added to the code package (such as Mimetic

operators [26]).

In three dimensions, the computational grid consists of $N \times M \times L$ grid points ($N \times M$ in two dimensions, N in one dimension). The wave function of the NLSE is discretized as

$$\Psi(x, y, z, t) \equiv \Psi_{i,j,k}^n, \quad (2)$$

where n is the current time step and i, j, k are the spatial positions on the grid. The time-step is denoted as \mathbf{k} and the spatial step-size is the same in each direction and defined by h . Therefore, $t = n\mathbf{k}$, $x = x_0 + ih$, $y = y_0 + jh$, and $z = z_0 + kh$. We define the end time of the simulation as $t_{\text{end}} = \mathbf{k} t_{\text{res}}$ where t_{res} is the number of time-steps taken.

3.1 Fourth-Order Runge-Kutta

In order to avoid (especially in three-dimensional problems) the need to solve a linear system and run nonlinear iteration routines at each time step, we use a fully explicit time-difference scheme. The classic four-stage, fourth-order Runge-Kutta (RK4) scheme [27] is the simplest single-stage explicit time-stepping that can be used for the NLSE directly (i.e, not using a real-imaginary staggered step as in Ref. [28]) and is (conditionally) stable [29]. The RK4 scheme can be written in algorithmic form as

$$\begin{aligned} 1) K_{\text{tot}} &= F(\Psi^n) & 6) K_{\text{tmp}} &= F(\Psi_{\text{tmp}}) & (3) \\ 2) \Psi_{\text{tmp}} &= \Psi^n + \frac{\mathbf{k}}{2} K_{\text{tot}} & 7) K_{\text{tot}} &= K_{\text{tot}} + 2 K_{\text{tmp}} \\ 3) K_{\text{tmp}} &= F(\Psi_{\text{tmp}}) & 8) \Psi_{\text{tmp}} &= \Psi^n + \mathbf{k} K_{\text{tmp}} \\ 4) K_{\text{tot}} &= K_{\text{tot}} + 2 K_{\text{tmp}} & 9) K_{\text{tmp}} &= F(\Psi_{\text{tmp}}) \\ 5) \Psi_{\text{tmp}} &= \Psi^n + \frac{\mathbf{k}}{2} K_{\text{tmp}} & 10) \Psi^{n+1} &= \Psi^n + \frac{\mathbf{k}}{6} (K_{\text{tot}} + K_{\text{tmp}}), \end{aligned}$$

where

$$F(\Psi) = \frac{\partial \Psi}{\partial t} = i [a \nabla^2 \Psi + (s |\Psi|^2 - V(\mathbf{r})) \Psi].$$

In NLSEmagic, the Laplacian of Ψ in $F(\Psi)$ is evaluated using either the CD or 2SHOC scheme. We denote the resulting combined scheme as RK4+CD and RK4+2SHOC respectively.

The RK4 has an error which is fourth-order in the time step ($O(k^4)$). In NLSEmagic, this error will always be much less than the error in computing the Laplacian of Ψ because, as we will see in Sec. 3.4, in order for the RK4 scheme to be stable $\mathbf{k} \propto h^2$, the proportionality constant depending on the dimensionality of the problem and spatial scheme. Thus, an error of $O(k^4)$ in our case is proportional to an error of $O(h^8)$, and since our spatial schemes are accurate only to $O(h^2)$ or $O(h^4)$, the error resulting from the RK4 is negligible.

3.2 Difference Schemes for the Laplacian Operator

NLSEmagic has two options for computing the Laplacian. The first is the standard second-order central difference scheme (CD), and the other is a two-step high-order compact scheme (2SHOC) which is fourth-order accurate [25].

The 2SHOC scheme allows for the use of coarser grids with equivalent accuracy to the CD scheme, or for use with simulations that need high accuracy. Usually, high-order schemes have a wide stencil, which are not suitable for parallel applications due to extra communication and/or memory latency. Also, the grid points near the boundary are difficult to deal with. The 2SHOC

schemes avoid these problems because in each step, the computation is compact (relying only on adjacent grid points). The drawbacks of the scheme are that they require the storage of an extra temporary variable and an increase in the number of floating point operations per grid point when compared to the standard fourth-order wide stencils. However, for our GPU implementation, the advantages of using the 2SHOC scheme outweigh the disadvantages.

In one-dimension, the two steps of the 2SHOC scheme are defined as

$$1) \quad D_i = \frac{1}{h^2} (\Psi_{i+1} - 2\Psi_i + \Psi_{i-1}), \quad (4)$$

$$2) \quad \nabla^2 \Psi_i \approx \frac{7}{6} D_i - \frac{1}{12} (D_{i+1} + D_{i-1}). \quad (5)$$

In two dimensions, the 2SHOC scheme is given by

$$1) \quad D_{i,j} = \frac{1}{h^2} \begin{array}{|c|c|c|} \hline & 1 & \\ \hline 1 & -4 & 1 \\ \hline & 1 & \\ \hline \end{array} \Psi_{i,j} \quad (6)$$

$$2) \quad \nabla^2 \Psi_{i,j} \approx -\frac{1}{12} \begin{array}{|c|c|c|} \hline & 1 & \\ \hline 1 & -12 & 1 \\ \hline & 1 & \\ \hline \end{array} D_{i,j} + \frac{1}{6h^2} \begin{array}{|c|c|c|} \hline 1 & & 1 \\ \hline & -4 & \\ \hline 1 & & 1 \\ \hline \end{array} \Psi_{i,j}, \quad (7)$$

and in three dimensions,

$$1) \quad D_{i,j,k} = \frac{1}{h^2} \left(\begin{array}{|c|c|c|} \hline & & \\ \hline & 1 & \\ \hline & & \\ \hline \end{array} \Psi_{i,j+1,k} + \begin{array}{|c|c|c|} \hline & 1 & \\ \hline 1 & -6 & 1 \\ \hline & 1 & \\ \hline \end{array} \Psi_{i,j,k} + \begin{array}{|c|c|c|} \hline & & \\ \hline & 1 & \\ \hline & & \\ \hline \end{array} \Psi_{i,j-1,k} \right), \quad (8)$$

$$2) \quad \nabla^2 \Psi_{i,j,k} \approx -\frac{1}{12} \left(\begin{array}{|c|c|c|} \hline & & \\ \hline & 1 & \\ \hline & & \\ \hline \end{array} D_{i,j+1,k} + \begin{array}{|c|c|c|} \hline & 1 & \\ \hline 1 & -10 & 1 \\ \hline & 1 & \\ \hline \end{array} D_{i,j,k} + \begin{array}{|c|c|c|} \hline & & \\ \hline & 1 & \\ \hline & & \\ \hline \end{array} D_{i,j-1,k} \right) \quad (9)$$

$$+ \frac{1}{6h^2} \left(\begin{array}{|c|c|c|} \hline & 1 & \\ \hline 1 & & 1 \\ \hline & 1 & \\ \hline \end{array} \Psi_{i,j+1,k} + \begin{array}{|c|c|c|} \hline 1 & & 1 \\ \hline & -12 & \\ \hline 1 & & 1 \\ \hline \end{array} \Psi_{i,j,k} + \begin{array}{|c|c|c|} \hline & 1 & \\ \hline 1 & & 1 \\ \hline & 1 & \\ \hline \end{array} \Psi_{i,j-1,k} \right).$$

The standard second-order central differencing in each dimension is simply given by step one of the 2SHOC schemes shown above.

3.3 Boundary Conditions

NLSEmagic includes three boundary condition options: 1) Dirichlet (D), 2) Modulus-Squared Dirichlet (MSD), and 3) Laplacian-zero (L0). For one-dimensional simulations, NLSEmagic1D also contains code for a one-sided (1S) boundary condition.

For the implementation of each boundary condition, it is necessary to define the time-derivative at a boundary point so that it can be implemented in each step of the RK4 scheme. In order to use the boundary conditions with the 2SHOC scheme, they additionally need to be expressed in terms of the Laplacian in order to compute proper boundaries in the first step of the 2SHOC.

Dirichlet boundary conditions are defined as when the value of the function at the boundaries is fixed to be a constant value, i.e.

$$\Psi_b = B, \quad (10)$$

where the subscript b represents a boundary point, and B is a real constant. The time-derivative formulation of this condition is simply

$$\frac{\partial \Psi_b}{\partial t} = 0. \quad (11)$$

For the NLSE, the Dirichlet condition in terms of the Laplacian of the wavefunction is

$$\nabla^2 \Psi_b = -\frac{1}{a}(s|\Psi_b|^2 - V_b)\Psi_b. \quad (12)$$

The Modulus-squared Dirichlet boundary condition is defined to be where the modulus-squared of the wavefunction at the boundary is set to a fixed constant, i.e.

$$|\Psi_b|^2 = B, \quad (13)$$

where B is a real constant. The MSD boundary condition is useful for many problems, especially those with a constant density background (such as those in Sec. 4). The time-derivative formulation of the MSD boundary condition can be approximated as [30]

$$\frac{\partial \Psi_b}{\partial t} \approx i \operatorname{Im} \left[\frac{1}{\Psi_{b-1}} \frac{\partial \Psi_{b-1}}{\partial t} \right] \Psi_b, \quad (14)$$

where $\frac{\partial \Psi_{b-1}}{\partial t}$ is precomputed using the internal finite-difference scheme. This reliance on the previously computed value of the time derivative of the interior point creates a synchronization issue in the CUDA codes of NLSEmagic (see Sec. 6 for details). The Laplacian form of the MSD for the NLSE is

$$\nabla^2 \Psi_b \approx \left[\operatorname{Im} \left(i \frac{\nabla^2 \Psi_{b-1}}{\Psi_{b-1}} \right) + \frac{1}{a} (N_{b-1} - N_b) \right] \Psi_b, \quad (15)$$

where

$$N_b = s|\Psi_b|^2 - V_b, \quad N_{b-1} = s|\Psi_{b-1}|^2 - V_{b-1}.$$

The Laplacian-zero boundary condition is defined as setting the Laplacian of the wavefunction at the boundary to zero. The time-derivative formulation of the L0 boundary condition for the NLSE is given by

$$\frac{\partial \Psi_b}{\partial t} = i(s|\Psi_b|^2 - V_b)\Psi_b, \quad (16)$$

while the Laplacian form is, by definition,

$$\nabla^2 \Psi_b = 0. \quad (17)$$

The boundary conditions included in NLSEmagic are chosen due to their relatively easy implementation and broad applicability. Additional boundary conditions could be added to the NLSEmagic codes if needed.

3.4 Stability

The finite-difference schemes used in NLSEmagic are fully explicit and, like most explicit schemes, are conditionally stable. This means that for a given spatial step size h , there exists a maximum value of the time-step \mathbf{k} that can be used without the scheme becoming unstable (i.e, blow-up). In Ref. [29], we performed a full linearized stability analysis for the schemes in NLSEmagic. The results are coded into the full research scripts of NLSEmagic where given the spatial step size h , the largest stable time-step \mathbf{k} is automatically set. However, from experience it is observed that the purely linear bounds found in Ref. [29] are very close to the linearized bounds, and since the bounds must be artificially lowered (due to nonlinear effects), using the purely linear bounds is often all that is needed (an exception to this would occur in the presence of large external potential values). Therefore, the basic driver scripts of NLSEmagic only compute the linear bounds.

The linear stability bounds of the RK4+CD scheme for the NLSE with $V(\mathbf{r}) = 0$ and $s = 0$ using Dirichlet or periodic boundary conditions are

$$\mathbf{k} < \frac{h^2}{d\sqrt{2}a}, \quad (18)$$

where d is the dimensionality of the problem (1, 2, or 3). The equivalent linear bound for the RK4+2SHOC scheme are given by

$$\mathbf{k} < \left(\frac{3}{4}\right) \frac{h^2}{d\sqrt{2}a}. \quad (19)$$

In the NLSEmagic driver scripts, these bounds are multiplied by 0.8 to avoid instability due to nonlinearities, boundaries, and/or the external potential.

4 Example Test Problems

Before describing the implementation of the NLSEmagic codes, we show here the example test problems that we will make use of in testing the speedup of the codes.

In one-dimension, we use the following exact co-moving dark soliton solution to the NLSE with $V(x) = 0$ and $s < 0$:

$$\Psi(x, t) = \sqrt{\left|\frac{\Omega}{s}\right|} \tanh \left[\sqrt{\left|\frac{\Omega}{2a}\right|} (x - ct) \right] \exp \left(i \left[\frac{c}{2a} x + \left(\Omega - \frac{c^2}{4a} \right) t \right] \right), \quad (20)$$

where c is the velocity of the soliton and Ω is the frequency. The soliton describes a localized curve in the modulus squared of Ψ which propagates without dispersion or dissipation amidst a constant density background. For our simulations we use $s = -1$, $a = 1$, $c = 0.5$, and $\Omega = -1$. We use a spatial grid-size of $h = 0.01$. The computed linear and linearized stability bounds for the RK4+CD scheme yield a maximum available time-step of $\mathbf{k} = 0.0070711$ and $\mathbf{k} = 0.0070534$ respectively. For the RK4+2SHOC scheme, the stability bounds are $\mathbf{k} = 0.0053033$ and $\mathbf{k} = 0.0052934$ respectively. Therefore, we use a time-step of $\mathbf{k} = 0.005$ for all simulations to ensure stability. A depiction of such a soliton within our simulations is shown in Fig. 3. The solution has constant modulus-square value at the boundaries (far from the soliton) and we therefore use the MSD boundary condition (14).

In two dimensions, we use an approximation to a steady-state dark vortex solution to the NLSE with $V(x) = 0$ and $s < 0$ given by

$$\Psi(r, \theta, t) = f(r) \exp[i(m\theta + \Omega t)], \quad (21)$$

where m is the topological charge of the vortex (in our case, we use $m = 1$) and where $f(r)$ is a real-valued radial profile which can only be found exactly through numerical optimization routines. Since we will be simulating the vortex solution on very large grids (up to nearly 2000×2000), inserting the interpolated exact numeric solution onto the grid can take a long time. Due to this, and since we are not interested in the exact solutions, we do not use the numerically exact profile but rather an approximation to it given by the initial condition of the one-dimensional dark soliton of Eq. (20) with $c = 0$ and $x > 0$.

We use a spatial step-size of $h = 0.25$. Although this allows for a maximum time step of approximately $\mathbf{k} = 0.016$, to allow for comparison between simulations of different dimensionality, we set the time-step to that of the one-dimensional examples, $\mathbf{k} = 0.005$. A depiction of the dark vortex within our simulations is shown in Fig. 3.

In three dimensions, we use an approximation to a dark vortex ring solution to the NLSE amidst a co-moving back-flow which causes the vortex ring to be a steady-state solution. The form of the initial condition in cylindrical coordinates is

$$\Psi(r, z, \theta, 0) = g(r, z) \exp \left[i \left(\frac{c}{2a} z \right) \right], \quad (22)$$

where $g(r, z)$ is taken to be a numerically-exact two-dimensional $m = 1$ dark vortex (which, since we only are using two-dimensional interpolations of resolutions up to 144×144 , is able to be formulated efficiently, unlike the largest two-dimensional example problem) at position $r = d$ in the r - z half-plane, where d is the radius of the vortex ring, and c is its intrinsic transverse velocity (given to asymptotic approximation in Ref. [31]). In our example, we choose $d = 5$ and use a spatial step of $h = 3/2$. Once again, for comparison purposes, we use a time-step of $\mathbf{k} = 0.005$ even though the scheme would be stable with a larger time-step (as large as 0.045). A depiction of the vortex ring within our simulations is shown in Fig. 3.

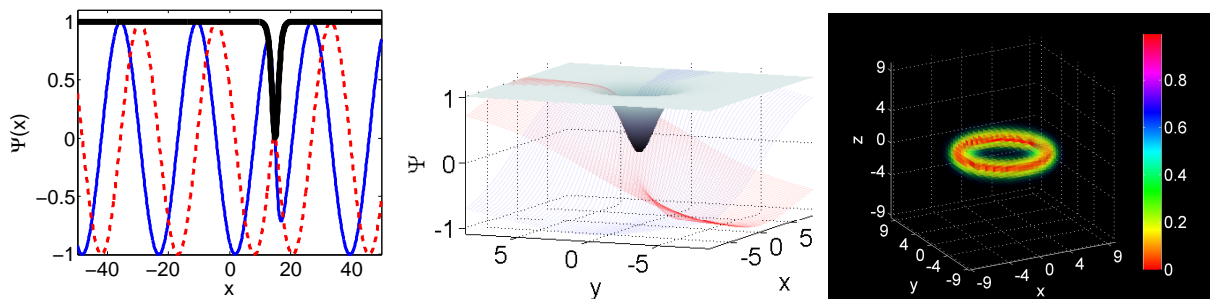


Figure 3: Left: Example of the one-dimensional dark soliton of Eq. 20 at time $t = 30$. The thin solid (blue) line and the thin dashed (red) line are the real and imaginary parts of Ψ respectively. The thick solid (black) line is the modulus-squared of the wave-function $|\Psi|^2$. The grid size here is $N = 1000$. Middle: Example of the approximate two-dimensional dark vortex of Eq. (21) at time $t = 0$. The (blue) and (red) mesh lines are the real and imaginary parts of Ψ respectively. The solid (gray) surface is the modulus-squared of the wave-function $|\Psi|^2$. The grid-size is $N = M = 70$. Right: Example of the approximate three-dimensional dark vortex ring of Eq. (22) at time $t = 0$. The image shows an inverted-volumetric rendering of the modulus-squared of Ψ . The grid size is $N = M = L = 29$.

5 Serial Code Implementations

We include the serial codes in NLSEmagic for two reasons. One, they allow us to calculate the speedup of the CUDA codes, as well as validate their simulation output. Second, the MEX serial codes are quite usable on their own, as they are very simple to install/compile and use, providing a good stepping stone for the user to get acquainted with the setup of NLSEmagic. The script integrators (included in the full-research version of NLSEmagic) are also useful as a platform for testing new numerical schemes and boundary conditions.

All NLSE integrators in NLSEmagic are set-up to simulate a ‘chunk’ of time-steps of the NLSE and return the resulting solution Ψ . The chunk-size is set based on the desired number of ‘frames’ (i.e. the number of times we want to have access to Ψ for plotting and analysis). For the serial integrators, this chunk-based approach is not necessary, but as we will see in Sec. 7.1, the chunk-based approach is very important for the CUDA integrators.

5.1 MATLAB Script Code Integrators

The script implementation of the NLSE integrators are used to quickly develop and test new methods, and are used for comparison of the speedup of the MEX integrators.

The script integrator code has two parts. The chunk of time-steps are computed in a `for` loop in the main driver script. The computations of $F(\Psi)$ in the RK4 scheme are done by calling a separate script file (`NLSExD_F.m`) which computes $F(\Psi)$ with the desired boundary conditions. All of the scripts utilize MATLAB vectorized operations wherever possible for efficiency.

The script integrators have been validated by numerous simulations of known solutions to the NLSE as well as its linear counterpart, the linear Schrödinger equation (LSE).

5.2 MATLAB MEX Code Integrators

The NLSEmagic serial MEX codes are stored in C source code files and integrate the NLSE for a given number of time steps and return the result to MATLAB.

When using a MEX file, it is important to handle complex values correctly. Since MEX files are written in C, one must either use a complex-number structure, or split the real and imaginary parts of the variables into separate vectors and write the numerical schemes accordingly. As shown in Ref. [9], for CUDA codes, using complex structures is less efficient than splitting the real and imaginary parts directly. Therefore, we split the values into real and imaginary parts and write the numerical scheme accordingly. Writing $F(\Psi)$ in this way we have

$$\begin{aligned} F(\Psi)_{i,j,k}^R &= -a \nabla^2 \Psi_{i,j,k}^I - s \left[(\Psi_{i,j,k}^R)^2 + (\Psi_{i,j,k}^I)^2 \right] \Psi_{i,j,k}^I + V_{i,j,k} \Psi_{i,j,k}^I \\ F(\Psi)_{i,j,k}^I &= a \nabla^2 \Psi_{i,j,k}^R + s \left[(\Psi_{i,j,k}^R)^2 + (\Psi_{i,j,k}^I)^2 \right] \Psi_{i,j,k}^R - V_{i,j,k} \Psi_{i,j,k}^R. \end{aligned} \quad (23)$$

Additional operations are straight-forward (for the split version of the MSD boundary condition, see Ref. [30]).

A MEX code in C is very similar to a regular C code, but uses MATLAB-specific interfaces for input and output data, and special MATLAB versions of memory allocation functions.

Instead of having a `main()` function as in pure C, the primary program is within a function called `mexFunction(nlhs, plhs[], nrhs, prhs[])`. The pointer `prhs[]` (pointer-right-hand-side) gives the C code access to the input data being sent from MATLAB, where `nrhs` is the

number of input variables (including arrays and scalars). The pointer `plhs[]` (pointer-left-hand-side) is used in allocating memory for output arrays and scalars, allowing the MEX code to return data to MATLAB.

Special MEX functions (`mxGetPr()`, `mxGetPi()` and `mxGetScalar()`) are used to extract the data from the `prhs[]` array of MATLAB inputs. The function `mxGetScalar()` is used to extract a scalar value while the functions `mxGetPr()` and `mxGetPi()` retrieve the pointer to the real and imaginary part of the selected input array respectively. If the input array is fully real (which can be often the case, especially for initial conditions), then the `mxGetPi()` is null-valued which causes a segmentation fault if accessed. To get around this problem, code has been added that checks to see if there is an imaginary part of the input array of Ψ (using `mxIsComplex()`), and if not, allocates an all-zero imaginary array manually (which is then freed at the end of the MEX code).

To allocate memory space for output arrays, the MEX functions `mxCreateDoubleMatrix()` (for 1D and 2D arrays) and `mxCreateNumericArray()` (for higher dimensionality arrays) are used to allocate memory space which is then pointed to by `plhs[i]`. This memory is then seen as a one-dimensional array by the C code, but in MATLAB will be the desired dimensionality.

In order to use the input and output arrays in C, proper indexing is essential. The MEX functions `mxGetN()` and `mxGetM()` are used to get the dimensions of one-dimensional and two-dimensional arrays (see below of three-dimensional array handling). However, because MATLAB stores arrays column-order, while C stores them row-order, the M value obtained from `mxGetM()` in the C code is actually the number of columns, while the N value obtained from `mxGetN()` is the number of rows (see Fig. 4). Therefore, the input array is seen by the MEX file as transposed

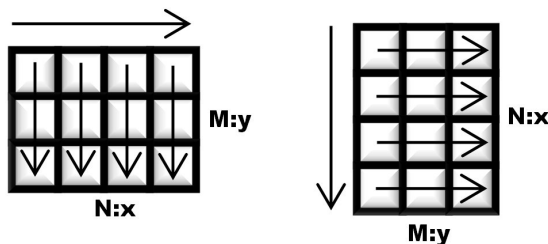


Figure 4: Representation of a two-dimensional array in MATLAB (left) and in C (MEX) (right). The arrows indicate the linear access pattern. The x and y dimensions shown are the x and y dimensions of the solution Ψ .

from the way it is seen in MATLAB (of course no actual transpose operation is performed in the MATLAB to C passing of arrays, only the order in which the different languages access the elements is different). Thus, while in MATLAB, the column length of the Ψ solution array is the number of grid points in the x -direction of Ψ and the row length is the number in the y -direction, inside the MEX file, this is reversed. (As will be seen in Sec. 6, this makes the ‘ x ’ CUDA grid dimension to be along the y -direction of the solution and vice-versa). The difference between the row-order access of C and the column-order access of MATLAB must be taken into account to correctly access the elements in an input array (here, called A). To access array element (i, j) (where $i \in [0, N - 1]$ and $j \in [0, M - 1]$) of array A in the MEX file, one uses `A[M*i+j]`, where M is the number of columns obtained from `mxGetM()`.

In three dimensions, the MEX functions `mxGetNumberOfDimensions()` and its counterpart `mxGetDimensions()` are used to get the dimensions of the 3D input arrays. The `mxGetDimensions()` returns an array of dimension lengths which, in our codes, are stored as L , M , and N . As in the

two-dimensional case, the access pattern differs in MATLAB and C. Once again, the M and N dimensions of the MATLAB array are seen by the MEX file as swapped (see Fig. 5). Thus, the

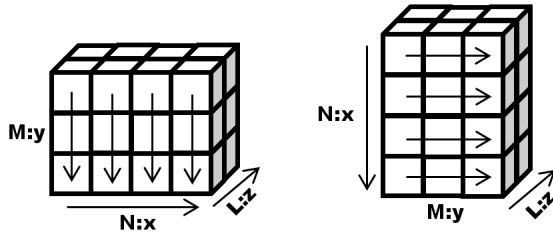


Figure 5: Representation of a three-dimensional array in MATLAB (left) and in C (MEX) (right). The arrows indicate the linear access pattern. The x , y and z dimensions shown are the x , y and z dimensions of the solution Ψ . Here, the z dimension maintains its orientation in the access pattern, while the x and y dimensions are transposed.

CUDA grid dimensions for x will be along the y -direction and vice-versa but the z grid dimension will correspond to the z -direction of the solution. To access array element (i, j, k) (where $i \in [0, L - 1]$, $j \in [0, N - 1]$, and $k \in [0, M - 1]$) of array A in the MEX file, one uses $A[M*N*i + M*j + k]$.

Within a MEX file, memory allocations and deallocations are performed using MEX comparable functions to the C functions `malloc()` and `free()` called `mxMalloc()` and `mxFree()`. The MEX function `mxMalloc()` allocates the desired memory in a MATLAB memory-managed heap. The advantage of using `mxMalloc()` instead of `malloc()` is that if a MEX file fails, or is interrupted during the program, MATLAB can handle and free the memory to better recover from the failure [32].

The compilation of a MEX file is performed within MATLAB using the `mex` command as `mex mymexcode.c`. The MEX compiler uses whatever C compiler on the current machine is selected by MATLAB. By default, MATLAB uses the included LCC compiler, but this can be changed using the `mex -setup` command in MATLAB. For the CUDA MEX codes on Windows, the compiler must be set to Microsoft Visual C++ while on Linux, the standard GCC compiler can be used. Thus for our serial MEX codes, we also use these compiler options. After a MEX file is compiled, the resulting binary file has a special extension which depends on the OS being used (`.mexw32` and `.mexw64` for 32-bit and 64-bit Windows respectively, and `.mexglx` and `.mexa64` for 32-bit and 64-bit Linux respectively).

Both single and double precision versions of the NLSEmagic serial MEX integrator codes have been developed in order to properly compare the single-precision versions of the CUDA MEX codes to their serial counterparts. The single precision MEX codes convert the input arrays to single precision (using the cast `float`), and then similarly converts the output arrays back to double precision (MATLAB’s native format) after the computation of the desire time steps.

5.3 Speedup of Serial MEX Codes

To illustrate the advantage of using MEX codes over script codes in MATLAB, we show timing results comparing the performance of the script integrators of NLSEmagic to the equivalent MEX codes using the example problems described in Sec. 4. As mention in Sec. 5.1, our script codes are sufficiently optimized by utilizing MATLAB’s built-in vector operations wherever possible (instead

of nested `for` loops).

We use the example solutions shown in Sec. 4 with an end-time of $t = 5$ and set the number of frames to 10. For all simulations we use double precision as it is MATLAB’s native format for the script codes. The simulations are performed for a total number of grid points of $\mathbf{N} = 10000$ to $\mathbf{N} = 1000000$. The results are shown in Fig. 6. We see that using MEX files is, on average, eight to fifteen times faster than the equivalent script codes. Although there is variation in the speedup (more for lower dimensions and variable over problem size), these variations are small and therefore the speedup of the MEX integrators can be considered approximately constant for all dimensions and problem sizes. Thus the serial MEX codes included in NLSEmagic are valuable on their own for those currently using script codes, especially since no special setup is needed to compile them and their use is straight-forward.

6 GPU-Accelerated CUDA MEX Code Integrators

In this section we describe in detail the design of the CUDA MEX integrators in NLSEmagic. Both single and double precision versions of all integrators are produced in order for the codes to be compatible with older GPU cards, as well as to increase performance when double precision accuracy is not required (as will be shown in Sec. 7, the single precision GPU codes can be much faster than double precision codes).

As mentioned in Sec. 2.2, there are two main sections of a CUDA code, the host code and the kernel codes. The host code is run on the CPU and is used to set up the problem, handle memory allocations and transfers to the GPU, and run the GPU kernel code. The kernels are the routines that are run on the GPU. A CUDA MEX code is almost identical to a standard CUDA C code except that its host code uses the MEX-specific functions described in Sec. 5.2 for input, output, and CPU memory allocation. However, since the kernel code is independent of the MEX interface, they are identical to kernels one would write for a pure CUDA C NLSE integrator code, and therefore can be easily ported to such a pure CUDA C code if desired.

The GPU-accelerated MEX routines in NLSEmagic are called from MATLAB in the exact same way as the serial MEX routines described in the previous section. That is, they have the same input and output parameters, and they integrate the NLSE over a specified number of time-steps (the chunk-size) before returning the current solution Ψ to MATLAB.

The basic outline of the integrators is that the input solution Ψ and potential $V(\mathbf{r})$ arrays obtained through the MEX interface are transferred to the GPU’s memory. Then, the desired number of time-steps are computed on the GPU using kernel functions, and the resulting solution is transferred back to the CPU memory, where it is outputted to MATLAB through the MEX interface.

Since the memory transfers from CPU to GPU and vice-versa are quite slow, the larger the number of time-steps the GPU computes before sending the solution back to the CPU (i.e. the larger the chunk-size), the better the expected speedup. In Sec. 7.1 we investigate this in detail for our simulations.

6.1 Specific Code Design for all Dimensions

We now discuss the details of the CUDA implementation which are the same for the one-, two-, and three-dimensional integrator codes. In the Sections that follow, we will discuss dimension-specific code design as well. We focus on the CUDA design aspects of the codes, and therefore do not mention any MEX interfaces (as they are all equivalent to the serial MEX codes previously

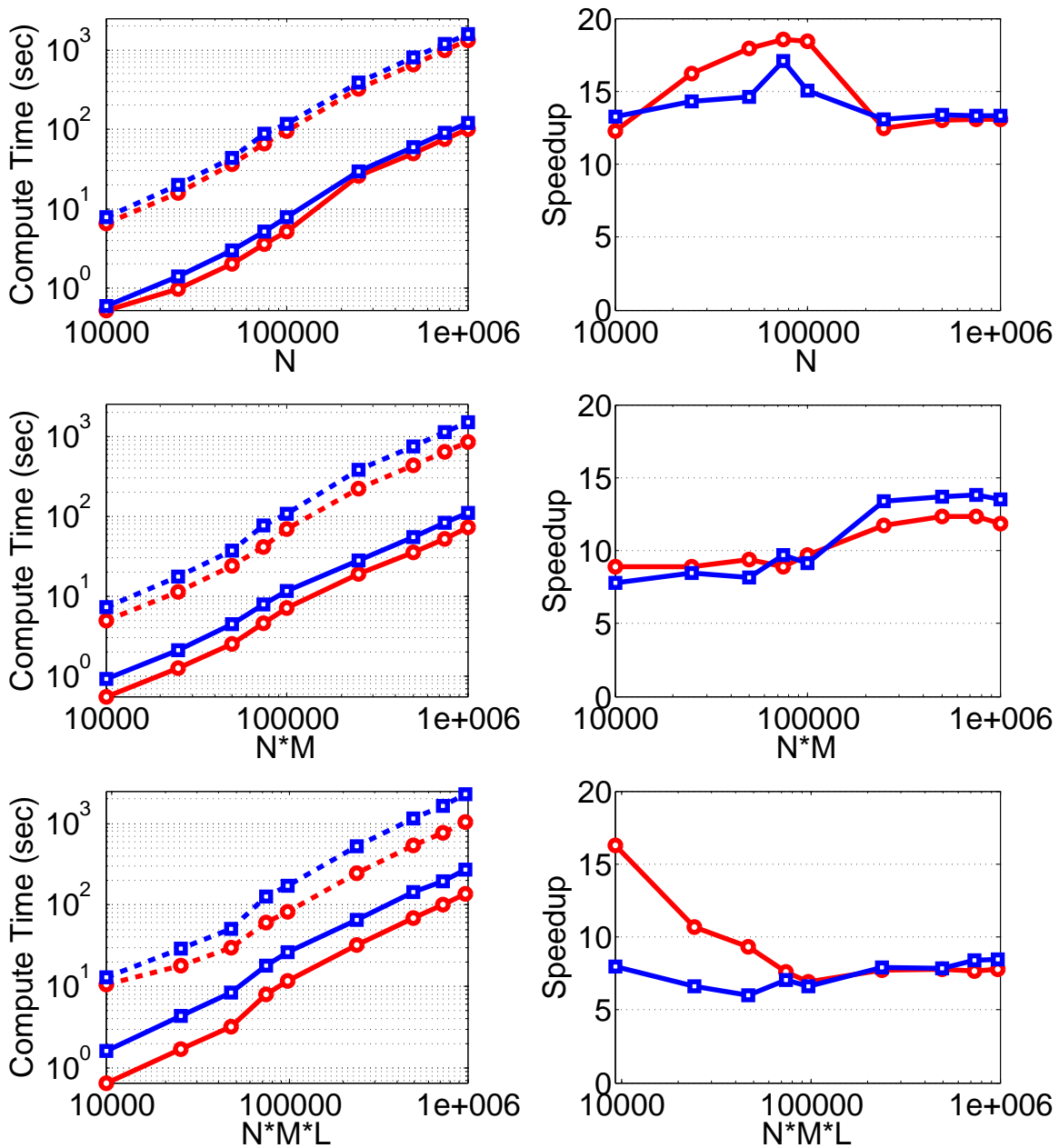


Figure 6: Timing results comparing script (dashed lines) and C MEX (solid lines) NLSE double-precision integrators for both the RK4+CD (red circles) and RK4+2SHOC (blue squares) schemes using the example problems of Sec. 4 with an end-time of $t = 5$ and a number of frames of 10. The simulations are performed for a total number of grid points of $N = 10000$ to $N = 1000000$. The results for the one-, two-, and three-dimensional codes are shown top to bottom. The left column displays the simulation times and the right column shows the speedup of the MEX codes.

described). Thus, we assume that the solution Ψ and potential $V(\mathbf{r})$ have already been obtained through the MEX interface along with all scalar parameters.

The first step in the code is to allocate arrays on the GPU’s global memory to store the solution, potential, and temporary arrays. This is accomplished by using the `cudaMalloc()` or the `cudaMallocPitch()` (see Sec. 6.3) function. Nine arrays the size of the total number of grid points \mathbf{N} are allocated when using the RK4+CD scheme, while eleven are needed for the RK4+2SHOC scheme. The arrays are composed of the real and imaginary parts of the solution vector Ψ , one array for the (real) external potential $V(\mathbf{r})$, and the real and imaginary parts of the three required temporary arrays for the RK4 algorithm (see below). For the RK4+2SHOC scheme, two additional arrays are needed to store the real and imaginary parts of the second-order Laplacian D . As mentioned in Sec. 5.2, it has been shown that splitting the real and imaginary parts of the solution arrays directly is more efficient than using a complex number structure [9].

The next step in the code is to transfer the solution Ψ and potential $V(\mathbf{r})$ arrays from the CPU’s memory to the memory locations allocated for them on the GPU’s global memory. This is done through the `cudaMemcpy()` or the `cudaMemcpy2D()` (see Sec. 6.3) function.

Before calling the compute kernel routines to integrate the NLSE, it is first necessary to define the CUDA compute-grid and block sizes for use in the kernel calls (a description of the grid, block, and thread logical structure was given in Sec. 2.2). The choice of block size is not trivial, and is dependent on the size of the problem and the GPU card being used. In order for a GPU to be most efficient, it requires that the problem has good *occupancy* on that specific card. This means that as many SMs are running as many SPs during the program simultaneously. Occupancy can have a large impact on performance. For example, if the number of threads in a block is smaller than the number of SPs per SM, not all SPs on the SMs will be utilized. On the other hand, if the block size is too big, the problem might fit into very few blocks, in which case the other SMs on the GPU will not be used at all! In NLSEmagic, the block sizes are chosen to provide efficiency for typical sized problems in each dimension (see following sections for details). The block size in each dimension is set using the `dimBlock()` function, whose result is stored in an intrinsic variable `dimBlock` which is a structure of type `dim3`.

The compute-grid size is found by taking the `ceil` of the length of the dimension of the specified problem array divided by the block size of that dimension. For example, the x -direction grid size in two dimensions would be found by `ceil(M/dimBlock.x)` where `dimBlock.x` is the x -direction block-size (it is important to note that, as per the discussion in Sec. 5.2, the x - and y -direction of the CUDA blocks are actually along the y - and x -direction of the solution Ψ within the C code respectively). Once the values for the grid dimensions are found, the grid is set up using the function `dimGrid()`, whose output is stored in an intrinsic variable called `dimGrid` which is a structure of type `dim3`.

Once the CUDA compute-grid and block sizes are set up, the code computes a chunk-size number of time-steps of the RK4 scheme using kernels which run on the GPU. The more computations a single kernel call performs, the better the performance of the GPU code. Therefore, we try to combine as many steps in the RK4 algorithm of Eq. (3) as possible. Since each compute block must be able to run independently of all the other blocks within a single kernel call, synchronization and race conditions (i.e, making sure a required result is computed before used) will limit how many steps of the RK4 can be combined. Each computation of $F(\Psi)$ in Eq. (3) (after the first one), for each grid point, requires the completed computation of Ψ_{tmp} of neighboring points from the previous step in order to compute the Laplacian of Ψ . Therefore, even with block-wide synchronizations, grid points along the boundary of compute-blocks will have no guarantee that the Ψ_{tmp} values it needs will have been computed yet or not (or even possibly already overwritten). Thus, multiple

separate kernels are required to run the steps in Eq. (3). When using the RK4+2SHOC scheme, an additional four kernels are required due to the same synchronization issues involving neighboring points needed from one step to the other (in this case the values of the Laplacian D in the first step of the 2SHOC scheme).

Although the computations of $F(\Psi)$ and D require separate kernels, the other steps in the RK4 algorithm *can* be combined with the kernels for $F(\Psi)$. Thus, the RK4 can be computed using only four kernels which contain steps 1–2, 3–5, 6–8, and 9–10 of Eq. (3). The only problem is that steps 3–5 and 6–8 can cause a synchronization issue. This is because step 5 (and 8) overwrites the Ψ_{tmp} values, which are the inputs to step 3 (and 6). Thus, when one block of threads finishes the step 3–5 computation, the adjacent block could still require the old values of Ψ_{tmp} along its neighboring edge to compute the Laplacian. To solve this, we introduce a storage array called Ψ_{out} which allows step 5 to output its values to Ψ_{out} so that the other blocks still have access to the original values of Ψ_{tmp} . Then in step 6, the code evaluates $F(\Psi_{out})$, while step 8 outputs to Ψ_{tmp} . Adding this vector does not increase the overall global memory storage requirements of the RK4 scheme because since the steps are now combined into four kernels, the K_{tmp} array does not need to be stored in global memory ever, and can instead be stored in a per-block shared memory. The RK4 algorithm can therefore be described on the GPU as

$$\begin{aligned}
1) k_{tmp} &= F(\Psi) & 7) k_{tmp} &= F(\Psi_{out}) & (24) \\
2) K_{tot} &= k_{tmp} & 8) K_{tot} &= K_{tot} + 2 k_{tmp} \\
3) \Psi_{tmp} &= \Psi + \frac{\mathbf{k}}{2} k_{tmp} & 9) \Psi_{tmp} &= \Psi + \mathbf{k} k_{tmp} \\
4) k_{tmp} &= F(\Psi_{tmp}) & 10) k_{tmp} &= F(\Psi_{tmp}) \\
5) K_{tot} &= K_{tot} + 2 k_{tmp} & 11) \Psi &= \Psi + \frac{\mathbf{k}}{6} (K_{tot} + k_{tmp}), \\
6) \Psi_{out} &= \Psi + \frac{\mathbf{k}}{2} k_{tmp},
\end{aligned}$$

where k_{tmp} is only stored in shared memory, while Ψ , K_{tot} , Ψ_{tmp} , and Ψ_{out} are stored in global memory (although during computation, they are transferred to shared memory as discussed below).

All four kernels in the computation of a RK4 step are computed using a single kernel function named `compute_F()`. One of its input parameters tells the kernel which step it is computing, and the corresponding computation is selected in a switch statement. For the 2SHOC scheme, an additional kernel is written named `compute_D()` which computes the D array before each call to `compute_F()`.

When a kernel is launched, the blocks in the compute-grid are scheduled to run on the MP, where each thread in the block runs the kernel. The first step in any kernel is to calculate the running thread’s index position based on the intrinsic variables described in Sec. 2.2. For example in one-dimension, the threads position in the block is given by `threadIdx.x` while its position in the grid is given by `blockIdx.x*blockDim.x + threadIdx.x`.

As discussed in Sec. 2.1, thread accesses to the per-block shared memory are much faster than accesses to the global memory of the GPU. Therefore if any array needed in the computations is accessed more than once by a thread in the block, it is worthwhile to copy the block’s required values of the array from global memory into shared memory. Then, after computing using the shared memory, the results can be copied back into global memory. Since shared memory is block-based, each thread in the block needs to copy its own value from the global array into the shared memory space (some threads may need to copy more than one value as we will show in Secs. 6.2, 6.3, and 6.4).

In `compute_F()`, five shared memory arrays are required (seven for the 2SHOC scheme). These consist of the real and imaginary parts of the Ψ input and the $F(\Psi)$ result (called k_{tmp} in the RK4 algorithm of Eq. (24)), as well as the potential array V . In the 2SHOC scheme, the real and imaginary parts of D are also stored in shared memory arrays. In the `compute_D()` kernel for the 2SHOC scheme, only two shared memory arrays are needed for Ψ .

Each thread in the block copies the global memory values into a shared memory array. Since the number of stream processors in the stream multi-processor that the block is being computed on almost always has less processors than the number of threads in the block, threads will typically not have access to all of the shared memory of the block after copying their own values. This is a problem because each thread has to access neighbor elements in the shared memory block for computation of the Laplacian of Ψ . Therefore, a `__syncthreads()` function is called after the copy which synchronizes all the threads in the block, ensuring that the entire shared-memory array of filled before using it for computing the Laplacian.

After the synchronization, the threads on the boundary of the block have to copy additional values into shared memory since they require accessing points which are beyond the block boundary due to the finite-difference stencil (see Secs. 6.2, 6.3, and 6.4 for details in each dimension). These transfers are not done before the block-synchronization because in CUDA, when a group of threads all need to perform the same memory transfer in a row, they are scheduled to do it in one chunk instead of randomly executed. Adding the boundary transfers before the synchronization may break up this pattern and cause the memory-copies not to be aligned for single-instruction copying.

After the transfers to shared memory are completed, the $F(\Psi)$ values are computed for all grid points within the boundaries of the solution Ψ . Once these interior points of $F(\Psi)$ are computed, threads which happen to be on the boundary of Ψ compute the boundary conditions of $F(\Psi)$. When using the MSD boundary condition, a block-synchronization is required using the routine `__syncthreads()` to be sure that the interior value of $F(\Psi)$ has been pre-computed (since it is necessary for the computation of the MSD condition). A problem exists if in any direction, the block is only one cell wide (since the interior point of $F(\Psi)$ will not be computed in that block). To avoid this problem in the most efficient way without adding extra error-checking code, the NLSEmagic driver scripts automatically adjust the solution grid size to ensure that this condition does not happen.

Once the boundary conditions of the $F(\Psi)$ array is completed, the kernel uses the result to compute the remaining sub-steps of the RK4 algorithm of that RK4 step. As mentioned above, which step in the RK4 is being computed is known through an input parameter to `compute_F()`.

For the 2SHOC scheme, the `compute_D()` kernel is very similar in structure to `compute_F()`. It first copies values of Ψ from global to shared memory (here only two shared memory arrays are required) including block-boundary values, and then computes D with its boundary conditions and stores the result in global memory.

After the desired number of RK4 time-steps (the chunk-size) have been completed, a call to `cudaDeviceSynchronize()` is made which ensures that all kernels are fully completed before continuing in the code (before the CUDA SDK 4.0, this function was called `cudaThreadSynchronize()`). This is required because although the CUDA GPU-to-CPU memory copies are designed to be implicitly synchronizing, in practice for large problems, we found that this was not completely reliable and we therefore explicitly synchronize the kernels. The current Ψ arrays are then transferred to the CPU using the `cudaMemcpy()` (or `cudaMemcpy2D()`) function. Finally, all the CUDA global memory spaces used are freed with `cudaFree()` and the MEX file returns the new value of Ψ back to MATLAB.

6.2 One-Dimensional Specific Code Design

In NLSEmagic1D, the CUDA compute-grid is set-up to be one-dimensional with a block size of 512 threads. Although for small problems a block size of 512 is not efficient in terms of occupancy (see Sec. 6), we feel that since one-dimensional problems typically run fast enough without any GPU-acceleration, the only time GPU-acceleration will be needed in one-dimensional problems is when the problem size is very large, in which case a block size of 512 will allow for good occupancy in most situations.

One of the key concerns in parallelizing finite-difference codes is the need for the cells on the edge of a compute-block to require values from their neighbor in another block. Since in the CUDA codes all threads in all blocks have equal access to global memory, there seems to be no problem with threads on the block boundaries. However, this is only true if the CUDA code only uses global memory (see Ref. [9] and [8], where the authors take this approach).

In order to greatly speedup the codes, it is vital to use the per-block shared memory in the computation whenever any global memory space is needed to be accessed by any thread more than once. The typical way to use shared memory is to have each thread in the block copy one value of Ψ (or D) and V from global memory into shared memory arrays which are the same size as the block size. Then the computation is done using the shared memory array, and at the end each thread stores the output into a global memory array. However, in this scenario, the block boundary cells do not have all their required Ψ (or D) values available in shared memory. There are a few different ways to deal with this. A simple solution is to have the block boundary threads directly access the required neighbor point(s) of Ψ (or D) from global memory when needed (as was done in Ref. [6]). Another solution is to set up the grid to overlap the boundary cells so that all threads copy values into shared memory as before, but only the interior threads of the block perform the computations, which can be performed using only shared memory. Through testing, we have found that this solution is not efficient because a large number of threads (the boundary threads) become idle after the memory copy.

Another solution is that instead of having the shared memory size be equal to the block size, the shared-memory size is allocated to be two cells greater than the block size. In the stage of the kernel where the threads transfer Ψ and V from global memory into shared memory, the boundary threads also transfer the neighboring points into the extra cell space at the boundary of shared memory. Therefore there are two global memory transfers performed by the block boundary cells instead of one. This process is depicted in Fig. 7. Later, in the computation part of the kernel, all threads can then compute using shared memory. Although this seems to be equivalent to the first method in terms of the number of global memory accesses (since in the first solution, the boundary cells access global memory twice as well – once to transfer their value to shared memory and once to access their required neighboring point), in practice, due to intricacies of the card hardware and software execution (for example, limiting the number of if-else branches), this method can be more efficient overall.

6.3 Two-Dimensional Specific Code Design

In two-dimensional CUDA codes, the CUDA API provides special global memory allocation and transfer routines called `cudaMallocPitch()` and `cudaMemcpy2D()`. The `cudaMallocPitch()` allocates a global memory space which is expected to be accessed in a two-dimensional pattern. It aligns the data with the card hardware, often padding the rows of the matrix. Therefore, the memory allocation function returns a pitch value which is used to access the element (i, j) as `pitch*i+j` instead of the usual `M*i+j`. The pitch value is also used in the `cudaMemcpy2D()` to transfer data

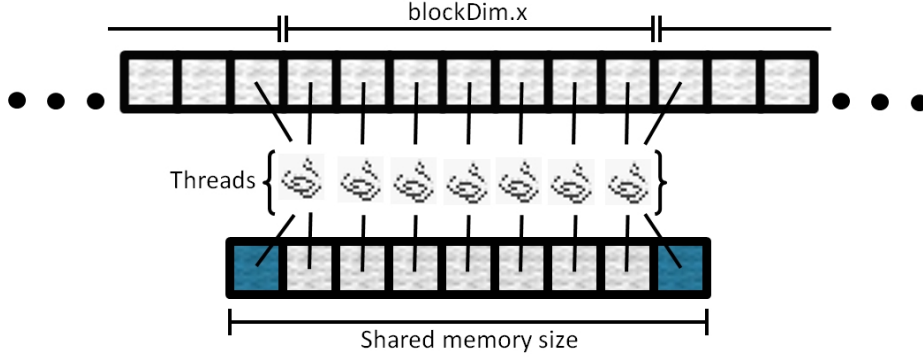


Figure 7: One-dimensional shared memory structure and transfer of global memory to shared memory. Note that the threads on the boundary of the block must perform two global memory retrievals into shared memory.

from the CPU to the GPU and vice-versa. The special two-dimensional routines are somewhat optional as one could also just use a standard linear memory transfer of the data and access the elements normally, but NVIDIA strongly recommends against it [12]. Therefore, NLSEmagic2D uses the specialized functions.

The CUDA compute-grid is set to be two-dimensional with two-dimensional blocks for easy indexing. The block size in NLSEmagic2D is set to be 16×16 . Based on performance tests, this is the best overall block size to use even though Fermi cards would allow a larger block size. The occupancy for a 16×16 block size is quite good even for smaller problems.

As in the one-dimensional code, the shared memory space is allocated to be two cells larger in width and height of the block size as shown in Fig. 8. The boundary threads once again grab the neighboring points in addition to their designated points from global memory during the shared-memory transfer process. For the CD scheme, the corner neighbor points are not needed, but for the 2SHOC scheme they are. This adds an additional global memory access on the corner threads (in addition the extra accesses from the other two neighboring points), making the corner threads copy up to four global values into shared memory.

When dividing the problem into CUDA blocks, the CUDA thread access ordering is an important consideration. The CUDA grid and block indexing is column-major ordered, with the ‘ x ’ direction along the columns and the ‘ y ’ direction is along the rows, and the threads are scheduled in that order. Thus, when copying arrays from global memory to shared memory, it is important that the access pattern of the memory being copied matches the access pattern of the thread scheduler [33]. Since C arrays are row-major, a shared memory array A should be allocated (counter-intuitively) as $A[\text{BLOCK_SIZEY}][\text{BLOCK_SIZEX}]$. The memory copy is then given as

$$A[\text{threadIdx.y}][\text{threadIdx.x}] = A_{\text{global}}[\text{pitch}*i+j],$$

where the position of the current thread within the solution array is given by

$$\begin{aligned} j &= \text{blockIdx.x} * \text{blockDim.x} + \text{threadIdx.x}, \\ i &= \text{blockIdx.y} * \text{blockDim.y} + \text{threadIdx.y}. \end{aligned}$$

Since in MATLAB (when using `meshgrid()` to form the x and y arrays of Ψ) the x direction of Ψ is along the rows of Ψ , and the y direction is along the columns, and when in the MEX file,

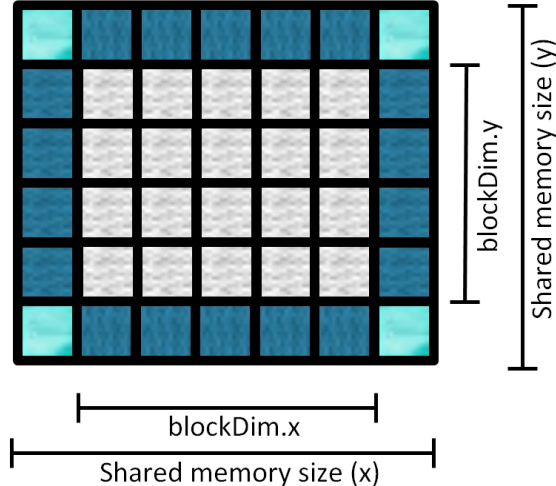


Figure 8: Two-dimensional shared memory structure. The threads on the boundary of the block must perform additional global memory retrievals into shared memory. Those on the corners perform a total of three transfers for the CD scheme, and four transfers for the 2SHOC (due to the required corner cells in the 2SHOC scheme). All other boundary threads perform two total transfers.

this is transposed, then, as mentioned in Sec. 5.2, the ‘ x ’ direction of the CUDA grid and blocks actually represent the y direction in Ψ and vice-versa. Therefore, in defining the grid size, we use $M/\text{dimBlock.x}$ for the x dimension of the grid and $N/\text{dimBlock.y}$ for the y even though N is the x -direction of Ψ and M is the y -direction. This is very important to remember when checking the MSD boundary condition grid requirement mentioned in Sec. 6.1. The thread access ordering described is not a trivial matter. In our tests, using the incorrect ordering can slow down the codes by a factor of almost a half!

6.4 Three-Dimensional Specific Code Design

In three dimensions, the CUDA API provides a hardware-optimized memory allocation and transfer functions similar to the two-dimensional ones mentioned in Sec. 6.3. However, the implementation of the three-dimensional functions (called `cudaMalloc3D()` and `cudaMemcpy3D()`) are not straightforward and requires making structures with information about the arrays, and passing the structures to the functions. Through testing of the two-dimensional NLSEmagic codes versus a naive two-dimensional implementation (without the specialized allocation and memory-copy), we did not observe any significant performance boost in using the hardware-optimized routines. Therefore, in order to keep things as simple as possible, the three-dimensional integrators of NLSEmagic3D do not use the specialized routines, and instead use the standard `cudaMalloc()` and `cudaMemcpy()` used in the one-dimensional codes and the global memory space in an array `A_global` for a point (i, j, k) is simply given by `A_global[N*M*i + M*j + k]`.

In Refs. [7] and [8], the three-dimensional finite-difference CUDA codes were set-up to do multiple two-dimensional sweeps and combining the results to form the three-dimensional derivatives. Thus, only a two-dimensional grid and block structure was used. This was done because the limit of 16KB of shared memory of the older GPUs was felt to be too limiting for using three-dimensional

blocks. However, in NLSEmagic3D, we use three-dimensional blocks which we note is efficient even when using older Tesla GPUs. On the Fermi cards, we have tested our code for various block sizes and have determined what are the most efficient block sizes for a typical problem size depending on the numerical method and precision being used (sometimes the choices are based on the shared memory size limitation of 48KB). For single precision, we use a block size of $16 \times 16 \times 4$ for the RK4+CD scheme and $12 \times 12 \times 4$ for the RK4+2SHOC. In double precision we use a block size of $10 \times 10 \times 5$ for the RK4+CD scheme and $8 \times 8 \times 6$ for the RK4+2SHOC.

An inherent difficulty with three-dimensional CUDA codes is that originally, even though blocks could be three-dimensional, the CUDA compute-grid could only be two-dimensional. Thus, there was no way to have a straight-forward extension from two-dimensional grids (i.e., to have a three-dimensional grid with each thread having an intrinsic `blockIdx.z` variable). This is an additional reason why previous studies (such as Refs. [7] and [8]) used two-dimensional slice algorithms.

Recently, NVIDIA has solved this problem as of the release of the CUDA SDK 4.0. With the new SDK, all Fermi based GPUs can now have a full three-dimensional grid structure. NLSEmagic3D was developed before this release, and therefore did not take advantage of this new feature. In order to allow NLSEmagic3D to be compatible with older Tesla-based GPUs, the integrators are not updated to use the new three-dimensional grids, but rather uses a custom logical three-dimensional structure on a two-dimensional CUDA compute-grid.

The three-dimensional problem grid is viewed as a series of three-dimensional slabs, each being one block high. These slabs are then seen as being placed side-by-side to create a two-dimensional grid of three-dimensional blocks as shown in Fig. 9. We thus have a true CUDA compute-grid

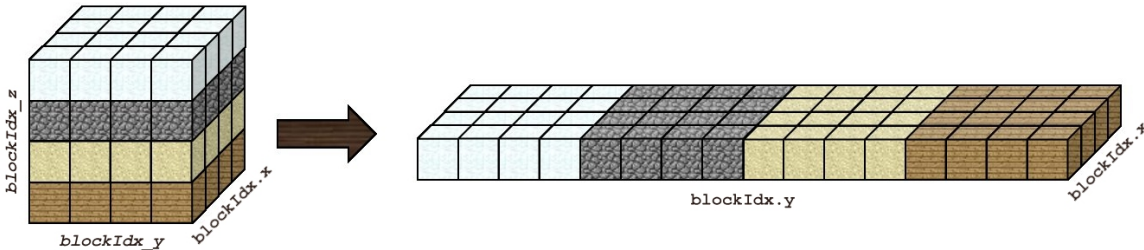


Figure 9: Logical block reordering for 2D CUDA grid from desired 3D grid structure.

which is two-dimensional with three-dimensional blocks, and a ‘virtual’ compute-grid which is a three-dimensional grid with three-dimensional blocks. In order to make the indexing as easy as possible within the true grid, we create new indexing variables per thread in order to use the full three-dimensional virtual CUDA compute-grid.

We note here that as in the two-dimensional case, the CUDA block/thread directions x , y , and z do not all correspond to those of Ψ . The CUDA block x -direction is actually along the y -direction of Ψ (M) and the CUDA block y -direction is actually along the x -direction of Ψ (N). The z -direction of both are equivalent. This is important to keep in mind for the computation of grid sizes and in checking the block requirements of the MSD boundary-condition in the driver scripts.

The first step in setting up the three-dimensional grid is that a variable

$$\text{gridDim}_y = \text{ceil}(N/\text{dimBlock}.y)$$

is set to represent the virtual CUDA y -direction grid size. Therefore, the true CUDA grid is defined to be

```
dimGrid(ceil(M/dimBlock.x),gridDim_y*ceil(L/dimBlock.z)).
```

The value of `gridDim_y` is passed into the kernels in order for the threads to have access to it. Inside the kernel, a new variable representing the thread's z -direction block position within the virtual three-dimensional grid called `blockIdx_z` is created defined as

```
blockIdx_z = blockIdx.y/gridDim_y
```

using integer division which acts as a floor function. The y -direction block position in the virtual grid is then found and stored in a new variable as

```
blockIdx_y = blockIdx.y - blockIdx_z*gridDim_y.
```

The `blockIdx_y` variable is therefore replacing the intrinsic `blockIdx.y` variable (which would give the y -direction block within the true CUDA grid). These new block position variables are depicted in Fig. 9.

Once the new indexing variables are created, the computation of the thread's designated position within the solution array is straight-forward as if there were a true CUDA three-dimensional grid. The values of the thread's indexes is therefore

```
k = blockIdx.x*blockDim.x + threadIdx.x,
j = blockIdx_y*blockDim.y + threadIdx.y,
i = blockIdx_z*blockDim.z + threadIdx.z,
```

where the thread is associated with the global memory position `A_global[N*M*i + M*j + k]`.

Once the older Tesla GPU cards are no longer in general use, direct 3D CUDA grids can be implemented in to the code, which, for our implementation, would be very straightforward (just setting up the grid based on M , N , and L directly and replacing the new thread indexes with the natural intrinsic ones).

As was the case in the two-dimensional codes, the dimensions of the shared memory space must be done in accordance with the thread access patterns in order to be efficient. (Note that this discussion is completely independent of the implementation of the three-dimensional compute-grid since, either way, three-dimensional blocks are being used and this issue is a block-wide problem). Since the threads are accessed in column order, first along x , then y , then z , it is important that the shared memory space be allocated in a way so that the memory copy is done as

```
A[threadIdx.z][threadIdx.y][threadIdx.x] = A_global[N*M*i + M*j + k].
```

As in the two-dimensional case, this correct ordering has a huge effect on performance (upwards of 50%) and is therefore vital.

As in the lower-dimensional integrator codes, NLSEmagic3D allocates the shared memory space to be two cells larger in each dimension than the block size. Thus, the threads on the block boundaries copy additional values from global memory into shared memory. For each required shared memory array, the interior threads copy one value, the threads along the faces of the block boundaries copy two values, the threads along the edges of the block boundary copy three values (four for Ψ in the 2SHOC scheme), and the threads on the corners of the block boundary have to copy four values (seven for Ψ in the 2SHOC scheme). The reason why there not even more copies necessary for the 2SHOC scheme is because the 2SHOC scheme never relies on the diagonal corner cells of Ψ or D , as it does not use a full 27-points stencil as seen in Eq. (9). Due to the large number of extra serialized memory copies for the boundary cell threads, the performance of the three-dimensional codes is not expected to be as good as the two-dimensional codes (this is indeed the case as shown in Sec. 7.4).

7 Speedup Results

Here we show the results of comparing the compute-time of the NLSEmagic CUDA integrators versus the serial MEX integrators. We choose to run the codes on a GeForce GTX 580 card (full specifications are listed in the appendix). Even though the double precision performance is artificially reduced in the GeForce cards, we show that this only effects our one-dimensional code, whereas our two- and three-dimensional codes have memory bottlenecks which make the reduced double precision performance negligible in practice. (After possible future optimization of the code, this may not be the case and it would be beneficial to run the codes on a more expensive Tesla compute-only GPU). Because the GeForce GPUs are many times cheaper than the Tesla (or Quadro) cards and the performance is not expected to be effected in a major way, we feel justified in running our codes on a GeForce card.

For all speedup tests, we use the example simulations as in Sec. 4 with an end-time of $t = 50$ and vary the total grid-size from about 1000 to 3,000,000. In each case we compute the computation time on the integrators, ignoring the small extra time required for generating the initial condition and outputting results.

Before computing the speedup results, it is first necessary to examine the effect of CPU–GPU memory transfers has on the performance of the integrators.

7.1 Chunk-size Limitations

As mentioned in Sec. 2.1, memory transfers between the CPU and GPU are very slow, and therefore it is best to compute as much as possible on the GPU before transferring the data back. For simulations where analysis results are cumulative, the entire simulation can be performed on the GPU with only two memory transfers (one at the beginning and one at the end of the computation). For most studies of time-dependent problems, it is desired or essential to have access to the computation data at regular intervals in order to save the data, display it for observation and animations, and to run intermediate analysis. However, the more times the data is needed by the CPU, the slower the code will perform. Therefore for NLSEmagic, the more frames the simulation is plotted, the slower the overall code will be.

In order to use the codes in the most efficient manner, it is necessary to see how much the simulation is slowed down as a function of the size of the chunk of time-steps performed by the CUDA integrator (which we designate as the *chunk-size*). Once a chunk-size is found which exhibits acceptable slow-down, the number of frames that the solution is viewable will be determined by the number of time-steps. Thus, if one wants more frames for a particular simulation, one could lower the time-step increasing the number of time-steps taken, or accept the reduced performance. Which of these two options is more efficient would have to be determined.

To see how the chunk-size affects performance of the NLSEmagic integrators, we run the examples described in Sec. 4 for various chunk-sizes and compare the compute-times. Since the performance of the codes due to chunk-size is not affected by the total number of time steps (as long as the number of time steps is larger than several chunk-sizes), we fix the end-time of the simulations to be $t = 5$ and the time-step to be $k = 0.005$ yielding 10,000 time-steps. We run the examples in each dimension with single and double precision for both the RK4+CD and RK4+2SHOC schemes for total grid sizes around 1000, 10,000, 100,000, and 1,000,000 (the two- and three-dimensional codes have slightly different resolutions due to taking the floor of the square- or cubed-root as the length in each dimension respectively). To eliminate dependency of the results on the specific compute times of the given problem (which would make comparison of different grid sizes difficult), for each chunk-size, we compare the compute times of the simulation to the fastest

time of all the simulations of that problem. As expected, this fastest time nearly always occurs when the chunk-size is equal to the number of time-steps. We thus compute a ‘slowdown’ factor as the time of the fastest run divided by the time of the other runs. This makes the results applicable to almost all simulations run with NLSEmagic. The results are shown in Fig. 10.

We see that in each case, the chunk-size has to be somewhat large for the codes to perform with top efficiency. Simulations with lower chunk-sizes can be done with acceptable slowdown based on the figures. In the higher dimensional cases, the larger the total grid size, the less the slowdown factor for a given chunk-size (In the one-dimensional case, the results are varied, with the lowest resolution tested outperforming the highest). Also, in general, it is seen that the higher-dimensional codes have less slowdown for a given chunk-size than lower-dimensional codes. Likewise, using the 2SHOC versus the CD scheme and double versus single precision, lower the slowdown for a given chunk-size as well. This is understandable since the more work the CUDA kernels are doing, the higher percentage of the total time is spent on computations compared to memory transfers to the CPU and back. In either case, when running NLSEmagic, it is best to first look up on Fig. 10 where the problem being simulated falls, and then choose an appropriate chunk-size to get the best performance out of the codes (within the simulation requirements).

7.2 One-Dimensional Speedup Results

For the one-dimensional results, we use the dark soliton solution in Sec. 4 with an end-time of $t = 50$. The solution is plotted five times during the simulation yielding a chunk-size of 5000, which is well over the efficiency requirements as discussed in Sec. 7.1. The soliton is simulated with a grid size which varies from $N = 1000$ to $N = 3,000,000$. Validation of the codes is done by comparing the solution to the known exact solution. The simulation compute-times and speedups compared to the serial MEX integrators are shown in Fig. 11 and Table 1. The best results are those of using the CD+RK4 scheme in single precision where we observed speedups around 90 for large grid sizes. Since, as was shown in Fig. 6, the serial integrators are about 12 times faster than the MATLAB script codes for those resolutions, the NLSEmagic CUDA MEX codes for the CD+RK4 scheme in single precision for large N are about *1000 times faster* than the equivalent MATLAB script code. In terms of actual time for the simulation tested, this would equate to taking roughly 30 seconds on the GPU versus 8 *hours* 20 minutes using the MATLAB script code.

Since the block size for the integrators was chosen to be 512, it is understandable that the compute time for the CUDA MEX codes stays quite low until resolutions of 10,000 or so. This is because the GPU being used has 16 MPs, and therefore resolutions up to 8000 can be computed in one sweep of the GPU MPs, while higher resolutions require multiple blocks to be computed on the same MP.

It is noticeable that the double-precision performance is almost half that of the single precision. This is partly due to what was mentioned in Sec. 2.1 that the GeForce cards have their double precision FLOP count artificially reduced by one quarter, making the FLOP count one-eighth that of the single precision performance. In addition, memory transfer is considered to be a large factor in code performance, and since double-precision variables take twice the memory space as single precision, a reduction in performance is understandable.

It is also apparent that the speedup when using the 2SHOC scheme is lower than the CD scheme. This is also understandable because in the 2SHOC scheme, kernels which only compute the D array (the standard second-order Laplacian) are needed, and they have a smaller amount of floating-point operations than the kernels which compute the full NLSE and RK4 step. Since the amount of computations in the D kernel is so small but the amount of required memory transfers

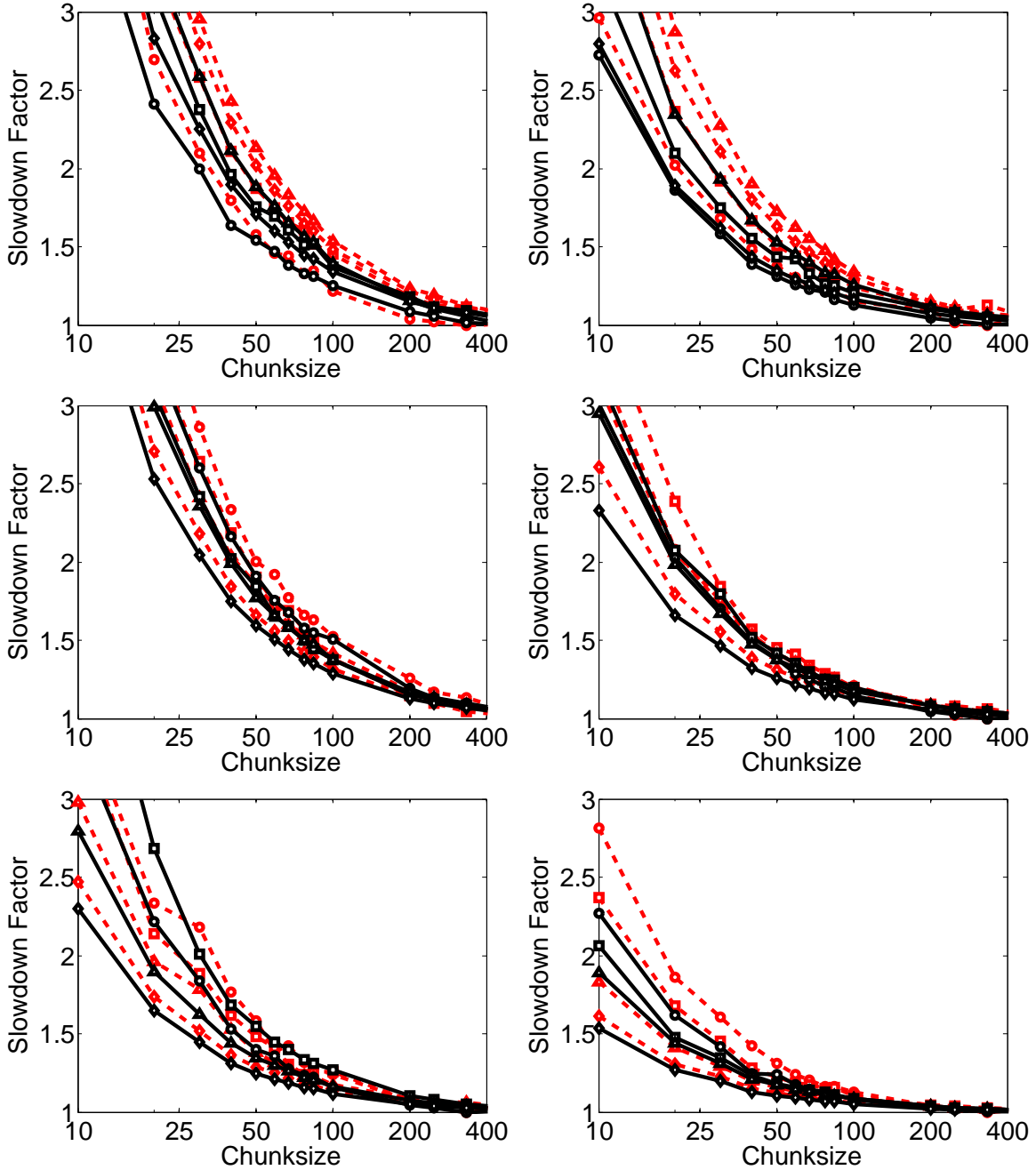


Figure 10: Slowdown factor versus chunk-size of the CUDA NLSEmagic integrators computed using the examples of Sec. 4 with an end-time of $t = 5$. The slowdown is how much slower the simulation is compared to the fastest possible simulation of chunk-size=time-steps (not shown). The results are shown for the RK4+CD and RK4+2SHOC (left and right respectively), for one-, two-, and three-dimensional simulations (top to bottom respectively), and for single and double precision (dashed and solid lines respectively). The circle, square, triangle, and diamond lines represent total grid-sizes of 1000, 10,000, 100,000, and 1,000,000 respectively.

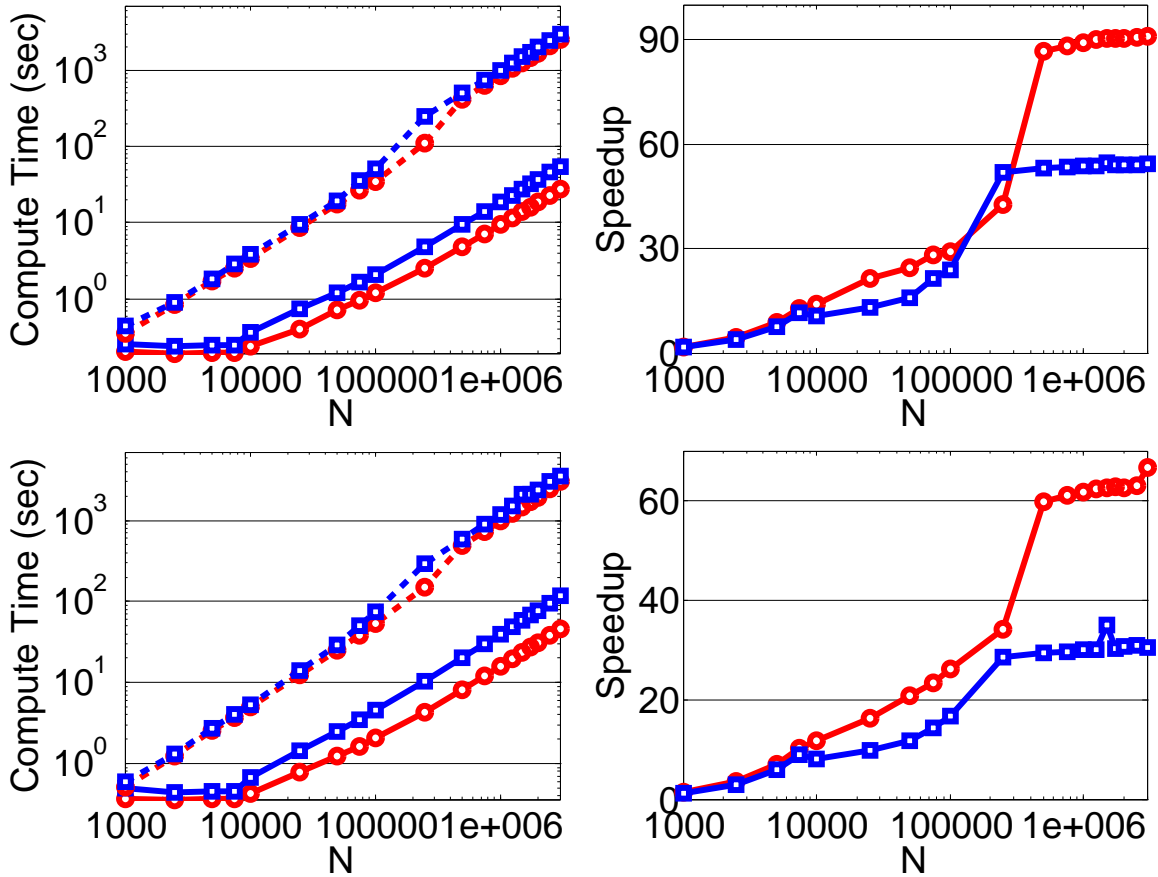


Figure 11: Computation times (left) and speedups (right) of the NLSEmagic1D CUDA MEX integrators (solid) versus the serial MEX integrators (dashed) for simulating the dark soliton solution described in Sec. 4 with an end-time of $t = 50$. The results are shown for both the RK4+CD scheme (top) and the RK4+2SHOC scheme (bottom) using both single (red circles) and double (blue squares) precision.

Table 1: Subset of the one-dimensional timing results from Fig. 11. The results are shown for the RK4+CD scheme in single precision (best results) and for the RK4+2SHOC in double precision (weakest results).

N	GPU Time (sec)		CPU Time (sec)		SPEEDUP	
	CD (s)	2SHOC (d)	CD (s)	2SHOC (d)	CD (s)	2SHOC (d)
1000	0.21	0.49	0.35	0.61	1.69	1.23
10000	0.24	0.67	3.39	5.38	14.07	7.99
100000	1.21	4.52	35.15	75.31	29.12	16.65
1000000	9.41	39.72	838.21	1192.27	89.08	30.01
3000000	27.65	117.32	2515.56	3581.40	90.98	30.53

is comparable to those of $F(\Psi)$, the speedup is smaller. As will be shown in Secs. 7.3 and 7.4, in higher dimensions, this issue is somewhat minimized due to the added number of points in the second-order Laplacian stencil (the speedup reduction is lowered from 27% in 1D to 16% in 3D in single precision, and from 45% to 0% in double precision).

A useful way of representing the timing results from Fig. 11 is to show the number of RK4 steps per second that the simulations took. The reason this can be useful is that typically, in a real problem using the RK4 scheme, one first chooses the domain size needed and the grid resolution desired (taking into account the spatial accuracy of the scheme, and the number of grid points needed to adequately resolve the solution). Once the spatial grid-spacing is chosen, one computes the maximum possible stable time-step. Now, based on the simulation time desired, the number of time-steps the simulation will take can be found. Therefore, knowing how many RK4 steps per second the codes are capable of running on the hardware will give a good estimate of the total time needed for the simulation. We show the number of RK4 steps per second from the simulations done for Fig. 11 in Fig. 12. An added benefit is that the results shown in Fig. 12 are independent of the

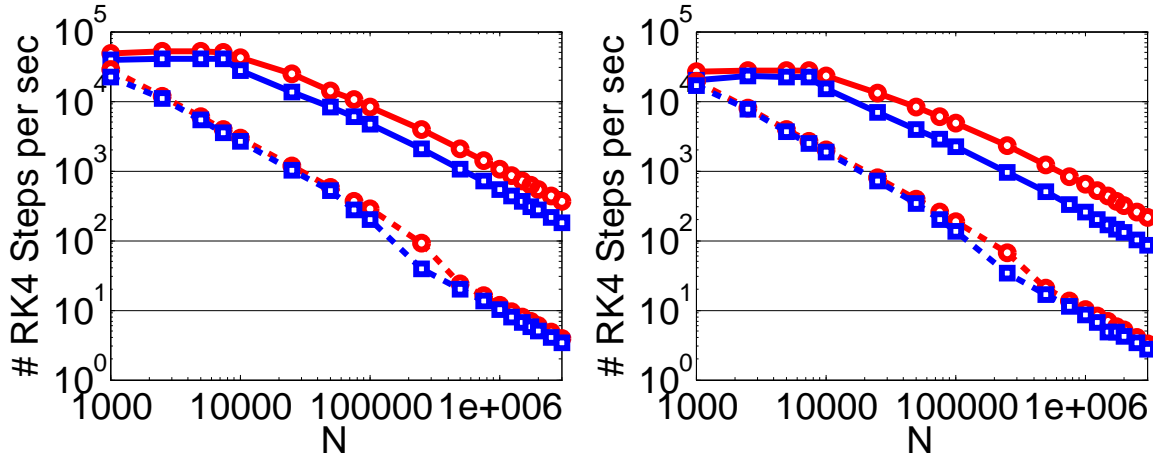


Figure 12: The number of RK4 time-steps per second for the simulations of Fig. 11 for the RK4+CD (left) and RK4+2SHOC (right) schemes. The additional figure properties are the same as those in Fig. 11.

total number of time-steps chosen for the simulations (keeping the chunk-size issues addressed in Sec. 7.1 in mind).

7.3 Two-Dimensional Speedup Results

For the 2D tests, we use the unoptimized steady-state dark vortex approximate solution of Sec. 4. Since there is no analytical solution to the dark vortex, and moreover, since we are using only an approximation of the true solution, we cannot record the error of the runs. Therefore, in order to validate the simulations, we displayed near-center cell data points for each frame and compared them with those from the output of the non-CUDA MEX codes, and checked that they were equivalent.

Like the one-dimensional tests, the solution is plotted five times during the simulation yielding a chunk-size of 5000, which is well over the efficiency requirements discussed in Sec. 7.1. The vortex solution is simulated with a total grid size which varies from about $\mathbf{N} = N * M \approx 1000$ to

$\mathbf{N} \approx 3,000,000$. The N and M dimensions are determined by taking the floor of the square-root of \mathbf{N} and are sometimes slightly altered due to the block requirements of using the MSD boundary condition (see Sec. 6.1).

The simulation compute-times and speedups compared to the serial MEX integrators are shown in Fig. 13 and Table 2. There is noticeably less speedup in the two-dimensional codes when compared to the speedup of the one-dimensional codes. A possible explanation for the cause of the reduced speedup is that in 2D there are many more boundary cells versus interior cells of the CUDA blocks (in fact, in 1D there are $O(1)$ while in a 2D square block, there are $O(N)$). Since, as described in detail in Sec. 6.3, block cell boundaries require additional global memory accesses (especially the corners), a decrease in performance was expected. Also, the number of total grid boundary points is much higher in 2D, in which case there are more threads computing boundary conditions than in 1D. This can cause less speedup in the codes since the MSD boundary condition requires an extra block-synchronization not needed in the internal scheme. Slightly better speedup results could be obtained by choosing a problem that has Dirichlet boundary conditions, but it is important to show results that apply to a more general range of applications.

It is important to note that despite the reduction in speedup of the two-dimensional codes, the speedup observed is still quite high, especially considering the cost of the GPU card. In fact, in the RK4+CD test of $\mathbf{N} = 1732^2 = 2999824$, the GPU code took about 40 seconds, while the serial MEX code took over 24 minutes. Based on the MEX speedups of Sec. 5.3, the equivalent MATLAB script code would be expected to take almost 5 *hours* to complete the same simulation. It is also important to note that resolutions for large \mathbf{N} values (where the best speedups are observed) are more common in two dimensions. Thus, the higher speedup results are expected to be more common in actual applications than those in one-dimension.

As explained in Sec. 7.2, it is useful to see the timing results displayed as the number of RK4 steps per second. In Fig. 14 we show the RK4 steps per second of the results from Fig. 13.

7.4 Three-Dimensional Speedup Results

For the 3D timings, we use the unoptimized approximate co-moving dark vortex ring of Sec. 4. As was the case in the 2D tests, we cannot record the error of the simulations. Therefore, to validate the simulations, we once again displayed near-center cell data points for each frame and compared them with those from the output of the non-CUDA MEX codes.

Like the one- and two-dimensional tests, the solution is plotted five times during the simulation yielding a chunk-size of 5000, which is once again well over the efficiency requirements discussed in Sec. 7.1. The vortex ring is simulated with a total grid size which varies from $\mathbf{N} = N*M*L \approx 10,000$ to $\mathbf{N} \approx 3,000,000$. The N , M , and L dimensions are determined by taking the floor of the third-root of \mathbf{N} and then slightly adjusted as needed to comply with the block requirements of using the MSD boundary condition mentioned in Sec. 6.1. Although for the one- and two-dimensional tests we started with simulations of size $\mathbf{N} \approx 1000$, in the three-dimensional case this was not possible due to the size of the vortex ring and the chosen spatial step-size (the vortex ring overlaps the grid boundaries when $\mathbf{N} \approx 1000$).

The simulation compute-times and speedups compared to the serial MEX integrators are shown in Fig. 15 and Table 3. We see that, once again, the higher dimensionality has reduced the speedup performance of the GPU codes. However, the decrease in speedup is less (in percent) than the decrease from the one- to the two-dimensional codes. A possible explanation is that the 3D codes have even more boundary cells in the CUDA block ($O(N^2)$) than the 2D case, and those cells require even more global memory accesses (as shown in Sec. 6.4, the 2SHOC scheme required

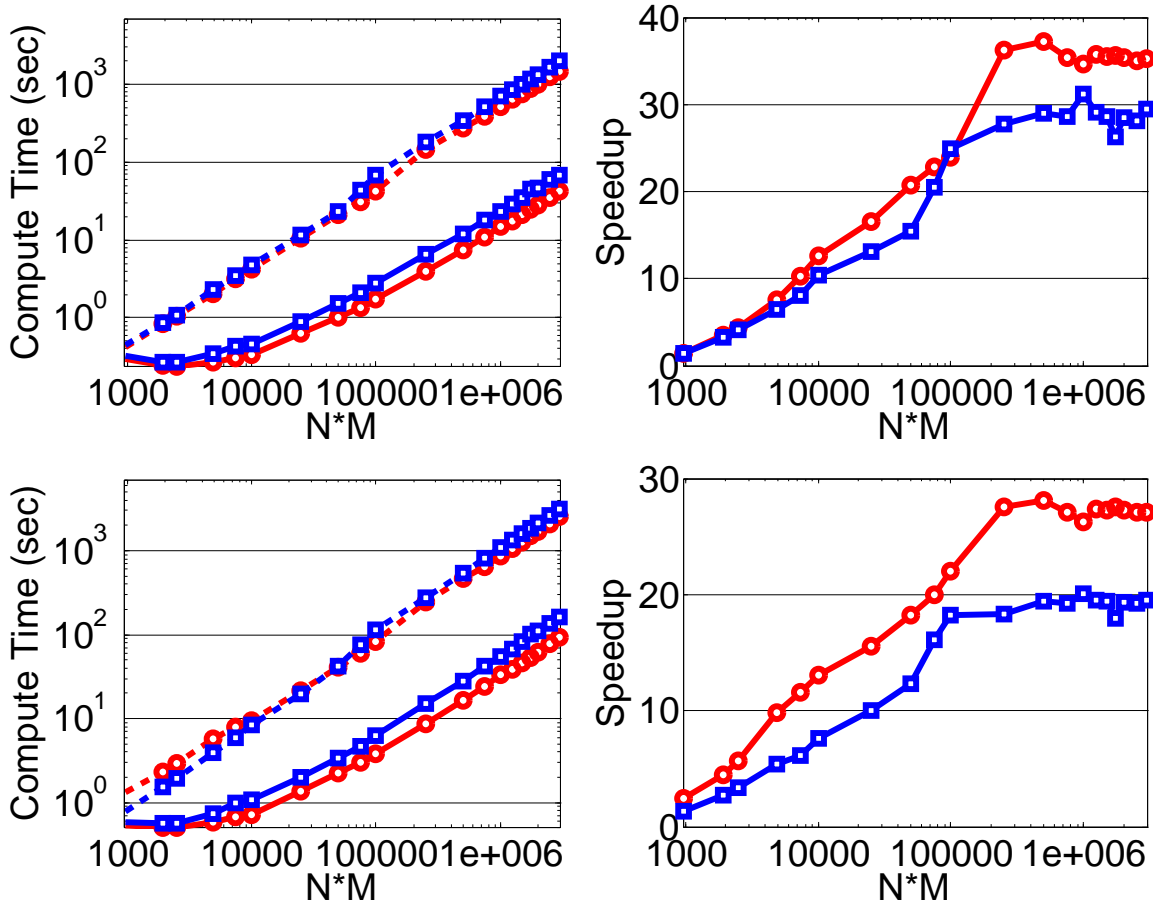


Figure 13: Computation times (left) and speedups (right) of the NLSEmagic2D CUDA MEX integrators (solid) versus the serial MEX integrators (dashed) for simulating the approximate dark vortex solution described in Sec. 4 with an end-time of $t = 50$. The results are shown for both the RK4+CD scheme (top) and the RK4+2SHOC scheme (bottom) using both single (red circles) and double (blue squares) precision.

Table 2: Subset of the two-dimensional timing results from Fig. 13. The results are shown for the RK4+CD scheme in single precision (best results) and for the RK4+2SHOC in double precision (weakest results).

$N * M$	GPU Time (sec)		CPU Time (sec)		SPEEDUP	
	CD (s)	2SHOC (d)	CD (s)	2SHOC (d)	CD (s)	2SHOC (d)
961	0.29	0.59	0.42	0.78	1.43	1.32
10000	0.34	1.09	4.25	8.35	12.61	7.65
99856	1.76	6.25	42.20	113.96	23.99	18.23
1000000	14.94	54.65	516.65	1094.72	34.59	20.03
2999824	42.15	162.79	1485.88	3173.51	35.26	19.49

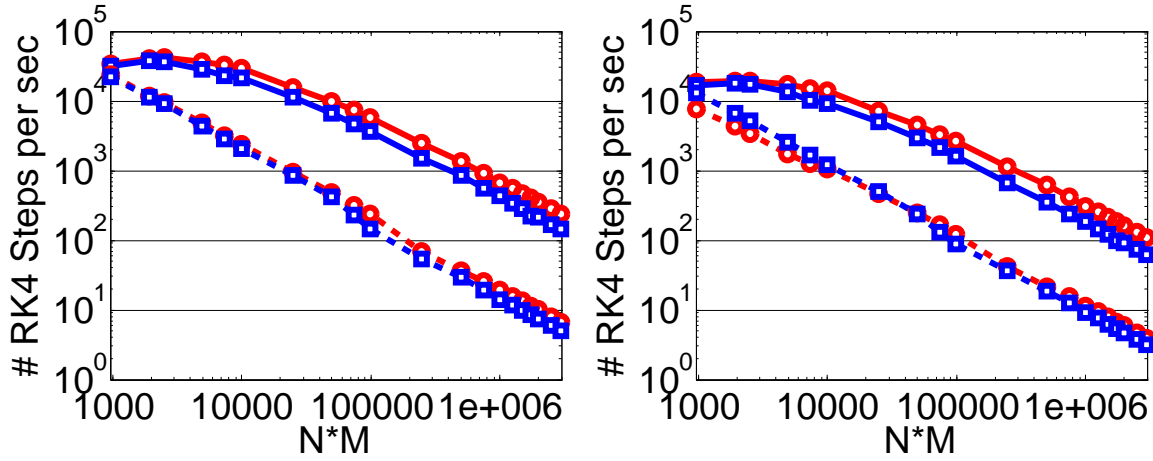


Figure 14: The number of RK4 time-steps per second for the simulations of Fig. 13 for the RK4+CD (left) and RK4+2SHOC (right) schemes. The additional figure properties are the same as those in Fig. 13.

Table 3: Subset of the three-dimensional timing results from Fig. 15. The results are shown for the RK4+CD scheme in single precision (best results) and for the RK4+2SHOC in double precision (weakest results).

$N * M * L$	GPU Time (sec)		CPU Time (sec)		SPEEDUP	
	CD (s)	2SHOC (d)	CD (s)	2SHOC (d)	CD (s)	2SHOC (d)
9261	0.59	2.00	4.85	14.17	8.29	7.10
97336	2.90	13.34	45.43	211.23	15.65	15.84
970299	31.85	131.74	733.46	2146.78	23.03	16.30
2985984	82.14	365.47	2106.77	6460.61	25.65	17.68

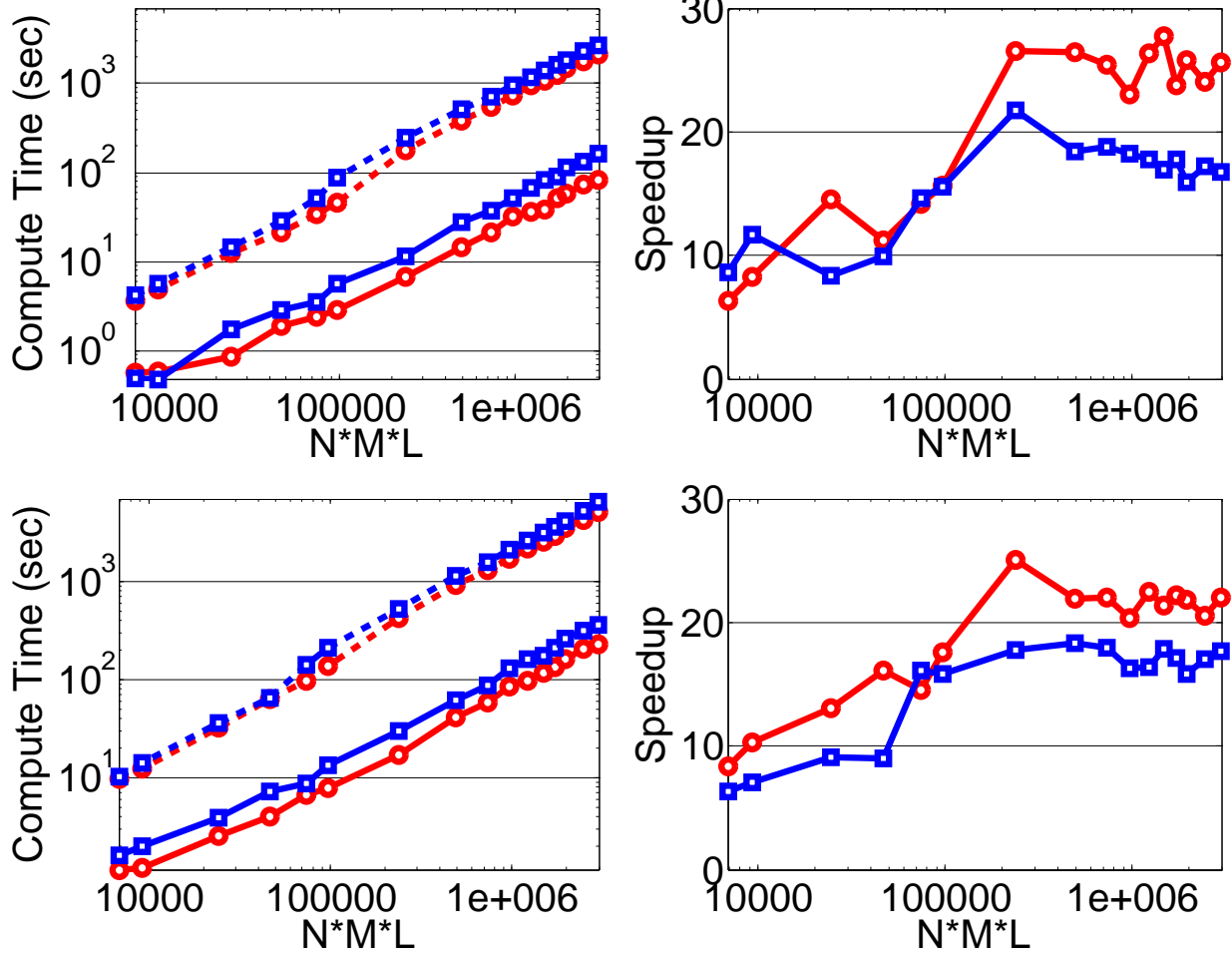


Figure 15: Computation times (left) and speedups (right) of the NLSEmagic3D CUDA MEX integrators (solid) versus the serial MEX integrators (dashed) for simulating the approximate dark vortex ring solution described in Sec. 4 with an end-time of $t = 50$. The results are shown for both the RK4+CD scheme (top) and the RK4+2SHOC scheme (bottom) using both single (red circles) and double (blue squares) precision.

up to 7 accesses for the corner cells). The additional number of grid boundary cells can also be a factor when using the MSD boundary condition as was explained in Sec. 7.3.

Despite the reduction in performance compared to the 2D results, the 3D codes still exhibit very good speedups, especially considering the cost and portability of the GPU card. For example, in the RK4+CD test of $\mathbf{N} = 149^3 = 2985984$, the GPU code took about 1 minute 20 seconds, while the serial MEX code took over 34 minutes. Based on the MEX speedups of Sec. 5.3, the equivalent MATLAB script code would take over 5 *hours* to complete the same simulation. Also, in 3D problems, even moderately resolved solutions require very large total grid sizes. Therefore, the larger speedups will be the most common in practical applications.

All the speedup tests presented in this paper were on grids which were nearly equal-sized in each dimension (i.e. $N \times N$ or $N \times N \times N$). Depending on the sizes, the block structure could be more or less optimized in terms of filling the edge blocks with more or less capacity. This explains why the speedups in 2D and (all the more so in 3D) are not smooth over changes in \mathbf{N} , but rather fluctuates. Therefore, certain specific grid sizes have the potential to be much more efficient. As an example, we have simulated a vortex ring solution in a grid with dimensions $87 \times 87 \times 203 \approx 1,500,000$ for an end-time of $t = 100$ and time-step size of $k = 0.03$ (yielding a chunk-size of only 56 which is on the low end of the efficiency requirements from Sec. 7.1) with the RK4+2SHOC scheme and the MSD boundary condition in double precision, and saw a speedup of over 26. This is much higher than the comparable speedup shown in Fig. 15 for the same total grid size and scheme. Thus, the actual speedup in any given problem may be higher than those shown in Fig. 15.

Like in the one- and two-dimensional cases, we show the timing results of Fig. 15 displayed as the number of RK4 steps per second (see Fig. 16).

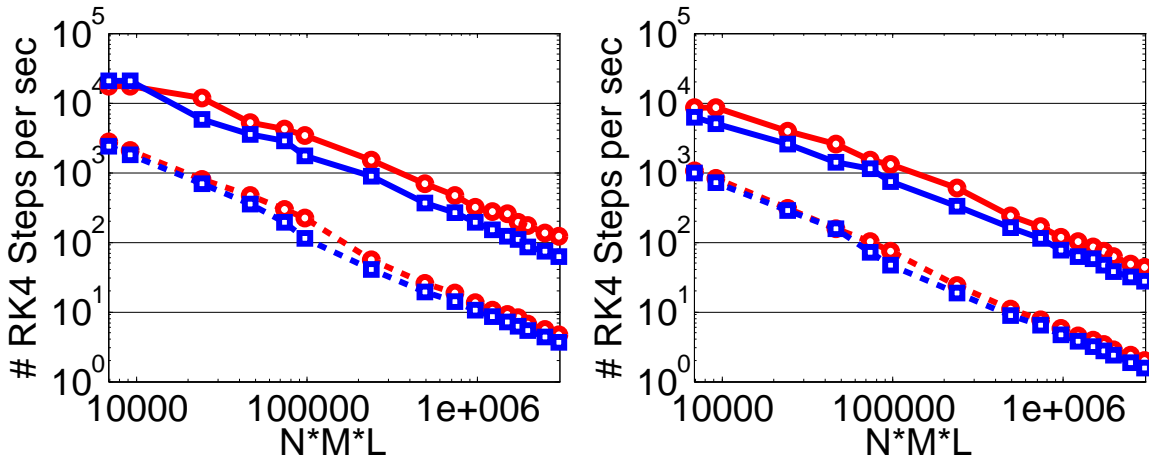


Figure 16: The number of RK4 time-steps per second for the simulations of Fig. 15 for the RK4+CD (left) and RK4+2SHOC (right) schemes. The additional figure properties are the same as those in Fig. 15.

8 The NLSEmagic Code Package

The codes described in this paper are packaged together and collectively named NLSEmagic: Non-linear Schrödinger Equation Multidimensional MATLAB-based GPU-accelerated Integrators using

Compact high-order schemes.

The basic NLSEmagic code package contains all the serial and CUDA MEX integrators. In addition, the package contains MATLAB script codes which are used as an example on how to use the integrators. These scripts are called `NLSEmagic1D.m`, `NLSEmagic2D.m`, and `NLSEmagic3D.m`.

Also available are full research MATLAB scripts which contain the initial conditions used in this paper, as well as code to visualize, analyze, and reproduce the timing results shown here. In addition, the full research scripts contain the script integrators used in the MEX speedup calculations of Sec. 5.3. The full research scripts are called `NLSE1D.m`, `NLSE2D.m`, and `NLSE3D.m`. They rely on additional script codes which are also provided in the packages.

In order to make using the codes as easy as possible, we also have made available pre-compiled binaries of the serial and CUDA MEX integrators for 32- and 64-bit Windows and Linux (coming soon).

The NLSEmagic code package is distributed free of charge at <http://www.nlsemagic.com>. The current website is shown in Fig. 17. The code packages and website contain documentation on how

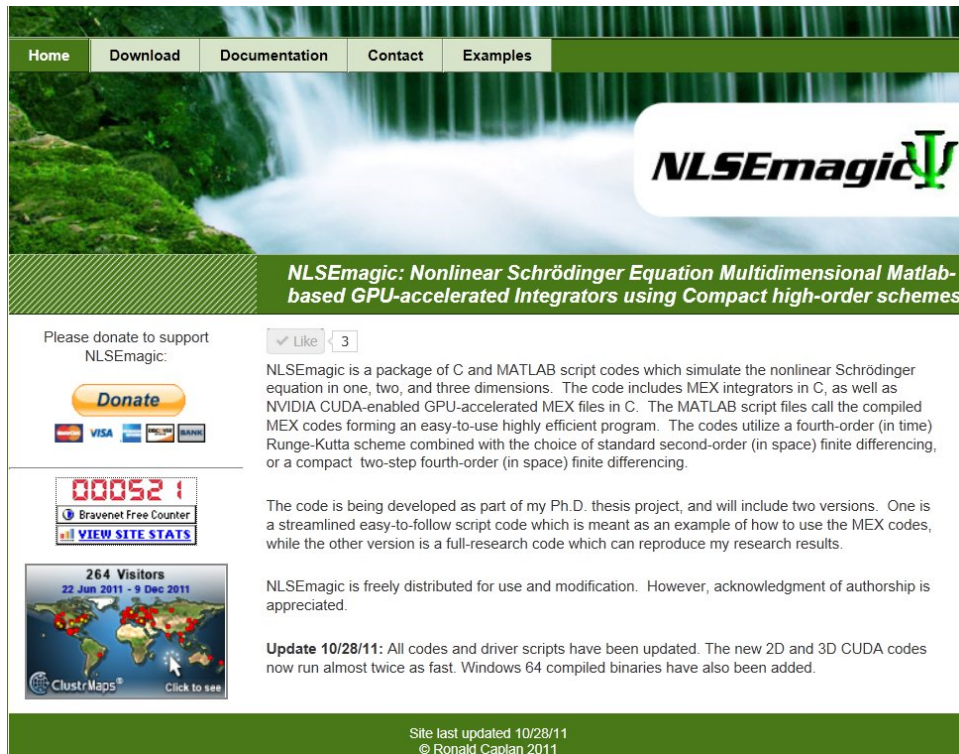


Figure 17: Screen-shot of www.nlsemagic.com, where all code packages of NLSEmagic are distributed free of charge.

to setup and install the various codes and run them. The setup required to compile the CUDA MEX codes is not trivial, and therefore we have striven to make our setup guide as user-friendly as possible. If recompiling the codes is not necessary for the user, the pre-compiled binaries are available and are more straight-forward to setup.

9 Conclusion

In this paper we have described the implementation of a new code package for simulating the multi-dimensional nonlinear Schrödinger equation utilizing GPU acceleration called NLSEmagic. The codes use an explicit finite-difference scheme using the fourth-order Runge-Kutta for the time-stepping and both a second-order central differencing and a two-step compact fourth-order differencing for the Laplacian. The codes are interfaced with MATLAB through MEX compiled C codes for ease of use. We have shown that the codes exhibit very good speedup results using an inexpensive GPU card. The NLSEmagic code package is available for free download at www.nlsemagic.com. We acknowledge the support of Professor Ricardo Carretero and NSF. We also would like to thank Mohammad Abouali for his advise on optimizing the CUDA codes.

A Specifications of CPUs and GPUs Used

Here we show the specifications of the GPU and CPU that were used for the results in this paper.

The CPU has the following relevant specifications:

Operating System:	MS Windows 7 Enterprise 64-bit
CPU Name:	Intel Core i3 540
CPU Clock Speed:	3.07 Ghz
Cores:	2
Threads:	4
L1 Data cache:	2 x 32 KB
L1 Instruction cache:	2 x 32 KB
L2 cache:	2 x 256 KB
L3 cache:	4 MB
DDR3 RAM:	4.0 GB
Memory Clock rate:	669 Mhz

Performance Information (Computed with QwikMark)

```
-----  
CPU Core Performance:      61 Gflop/s  
Memory Bandwidth:         6 GB/s
```

The GPU has the following relevant specifications:

GPU Name:	GeForce GTX 580 (EVGA)
CUDA Driver Version / Runtime Version:	4.1 / 4.1
CUDA Capability Major/Minor version number:	2.0
Total amount of global memory (GDDR5 RAM):	1536 MB
(16) Multiprocessors x (32) CUDA Cores/MP:	512 CUDA Cores
GPU Clock Speed:	1.59 Ghz
Memory Clock rate:	2025.00 Mhz
L2 Cache Size:	786432 bytes
Total amount of shared memory per block:	49152 bytes
Total number of registers available per block:	32768

Maximum number of threads per block:	1024
Concurrent copy and execution:	Yes with 1 copy engine
Run time limit on kernels:	Yes
Concurrent kernel execution:	Yes
Device has ECC support enabled:	No

Performance Information (Computed with CUDA-Z)

Memory Copy

Host Pinned to Device:	596.208 MB/s
Host Pageable to Device:	532.289 MB/s
Device to Host Pinned:	594.033 MB/s
Device to Host Pageable:	531.315 MB/s

GPU Core Performance

Single-precision Float:	1622440 Mflop/s
Double-precision Float:	204026 Mflop/s
32-bit Integer:	814731 Mflop/s
24-bit Integer:	813770 Mflop/s

References

- [1] L. Debnath. *Nonlinear Partial Differential Equations for Scientists and Engineers*. Birkhauser Boston, New York, New York, 2 edition, 2005.
- [2] P. G. Kevrekidis, D. J. Frantzeskakis and R. Carretero-González. *Emergent Nonlinear Phenomena in Bose-Einstein Condensates: Theory and Experiment*, volume 45. Springer Series on Atomic, Optical, and Plasma Physics, 2008.
- [3] R. M. Caplan, R. Carretero-González, P.G. Kevrekidis and Q. E. Hoq. Azimuthal modulational instability of vortices in the nonlinear Schrödinger equation. *Opt. Comm.*, **282** (2009) 1399–1405.
- [4] S.E. Krakiwsky, L.E. Turner and M.M. Okoniewski. Graphics processor unit GPU acceleration of finite-difference time-domain (FDTD) algorithm. In *Circuits and Systems, 2004. ISCAS '04. Proceedings of the 2004 International Symposium on*, volume 5, pages 265–268, 2004.
- [5] S. Adams, J. Payne and R. Boppana. Finite difference time domain (FDTD) simulations using graphics processors. *HPCMP Usr. Grp. Conf.*, (2007) 334–338.
- [6] A. Balevic, L. Rockstroh, A. Tausendfreund, S. Patzelt, G. Goch and S. Simon. Accelerating simulations of light scattering based on finite-difference time-domain method with general purpose GPUs. In *Computational Science and Engineering, 2008. CSE '08*, pages 327–334, 2008.
- [7] Paulius Micikevicius. 3D finite difference computation on GPUs using CUDA. In *Proceedings of 2nd Workshop on General Purpose Processing on Graphics Processing Units, GPGPU-2*, pages 79–84, New York, NY, USA, 2009. ACM.

- [8] David Michéa and Dimitri Komatitsch. Accelerating a three-dimensional finite-difference wave propagation code using GPU graphics cards. *Geo. J. Inter.*, **182**, 1 (2010) 389–402.
- [9] K. A. Hawick and D. P. Playne. Numerical simulation of the complex Ginzburg-Landau equation on GPUs with CUDA. (2010) CSTN-070.
- [10] Mathworks. MATLAB GPU computing with NVIDIA CUDA-enabled GPUs. (2011).
- [11] NVIDIA. White paper: Accelerating MATLAB with CUDA using MEX files. (2007).
- [12] NVIDIA. NVIDIA CUDA C programming guide 4.0. (2011).
- [13] NVIDIA. White paper: NVIDIA's next generation CUDA compute architecture: Fermi. (2009).
- [14] NVIDIA. Why choose tesla. <http://www.nvidia.com/object/why-choose-tesla.html>, (2011).
- [15] John E. Stone, David Gohara and Guochun Shi. OpenCL: A parallel programming standard for heterogeneous computing systems. *Comp. in Sci. and Engi.*, **12** (2010) 66–73.
- [16] Khronos Group. OpenCL overview. <http://www.khronos.org/opencl/>, (2011).
- [17] *Evaluating Performance and Portability of OpenCL Programs*, 2010.
- [18] Jianbin Fang, Ana Lucia Varbanescu and Henk Sips. A comprehensive performance comparison of CUDA and OpenCL. In *Parallel Processing (ICPP), 2011 International Conference on*, pages 216–225, 2011.
- [19] Kamran Karimi, Neil G. Dickson and Firas Hamze. A performance comparison of CUDA and OpenCL. *ArXiv e-prints*, (2010) arXiv:1005.2581.
- [20] Gabriel Martinez, Wu-chun Feng and Mark Gardner. CU2CL: A CUDA-to-OpenCL translator for multi- and many-core architectures. Technical report, Virginia Tech, 2011.
- [21] The Portland Group. PGI CUDA-x86: CUDA programming for multi-core CPUs. *PGInsider*, **2**, 4 (2010) a1.
- [22] John Stratton, Sam Stone and Wen-mei Hwu. *MCUDA: An Efficient Implementation of CUDA Kernels for Multi-core CPUs*, volume 5335 of *Lecture Notes in Computer Science*. Springer Berlin / Heidelberg, 2008.
- [23] J. S. Vetter, R. G., J. Dongarra, K. Schwan, B. Loftis, S. McNally, J. Meredith, J. Rogers, P. Roth, K. Spafford and S. Yalamanchili. Keeneland: Bringing heterogeneous GPU computing to the computational science community. *Comp. in Sci. and Engi.*, **13**, 5 (2011) 90–95.
- [24] The Portland Group. PGI accelerator compilers. <http://www.pgroup.com/resources/accel.htm>, (2011).
- [25] R. M. Caplan and R. Carretero-González. A Two-Step High-Order Compact Scheme for the Laplacian Operator and its Implementation in an Explicit Method for Integrating the Nonlinear Schrödinger Equation. *ArXiv e-prints*, (2011) arXiv:1109.1027.

- [26] J.E. Castillo, J.M.Hymanb, M. Shashkov and S. Steinberg. Fourth- and sixth-order conservative finite difference approximations of the divergence and gradient. *Appl. Num. Math.*, **37** (2001) 171187.
- [27] J.C. Butcher. A history of Runge-Kutta methods. *Appl. Num. Math.*, **20**, 3 (1996) 247–260.
- [28] M. M. Cerimele, M. L. Chiofalo, F. Pistella, S. Succi and M. P. Tosi. Numerical solution of the Gross-Pitaevskii equation using an explicit finite-difference scheme: An application to trapped Bose-Einstein condensates. *Phys. Rev. E*, **62** (2000) 1382–1389.
- [29] R. M. Caplan and R. Carretero-González. Numerical stability of explicit runge-kutta finite difference schemes for the nonlinear Schrödinger equation. *arXiv:1107.4810*, (2011).
- [30] R. M. Caplan and R. Carretero-González. A modulus-squared Dirichlet boundary condition for time-dependant complex partial differential equations and its application to the nonlinear Schrödinger equation. *ArXiv e-prints*, (2011) arXiv:1110.0569.
- [31] P. H. Roberts and J. Grant. Motions in a Bose condensate I. The structure of the large circular vortex. *J. Phys. A: Gen. Phys.*, **4** (1971) 55–72.
- [32] T.A. Davis. *MATLAB Primer, Eighth Edition*. CRC Press, 2010.
- [33] B. Jang, D. Schaa, P. Mistry and D. Kaeli. Exploiting memory access patterns to improve memory performance in data-parallel architectures. *IEEE Trans. on Par. and Dist. Sys.*, **22**, 1 (2011) 105 – 118.